Université de Montréal

Deux études spectroscopiques d'objets évolués et compacts

par

Caroline Pereira

Département de physique

Faculté des arts et des sciences

Mémoire présenté à la Faculté des études supérieures

en vue de l'obtention du grade de

Maître ès sciences (M.Sc.)

en physique

Août, 2005

Université de Montréal

Faculté des études supérieures

Ce mémoire intitulé:

Deux études spectroscopiques d'objets évolués et compacts

présenté par:

Caroline Pereira

a été évalué par un jury composé des personnes suivantes:

Gilles Fontaine,	président-rapporteur
Pierre Bergeron et François Wesemael,	directeur de recherche
Pierre Brassard,	membre du jury

Mémoire accepté le: 16/09/05

Sommaire

Nous présentons deux études spectroscopiques d'objets évolués et compacts. D'abord, nous soulignons la découverte de variations spectroscopiques dans la naine blanche de type spectral DAB, GD 323. L'analyse simultanée de spectres visibles de GD 323 et de PG 1234+482, une DA non-variable, nous permet de trouver des variations quasi-périodiques des raies d'hydrogène et d'hélium. De plus, les raies d'hydrogène varient hors-phase avec la raie He I λ4471. Cette découverte suggère un modèle d'atmosphère avec des abondances inhomogènes plutôt que celui d'une atmosphère stratifiée. Ensuite, nous vérifions la cohérence entre les paramètres atmosphériques dérivés à partir de spectres visibles et les observations dans l'ultraviolet lointain pour un échantillon de neuf sous-naines. Nous avons calculé une grille de modèles d'atmosphères hors-ETL d'hydrogène pur, et une incluant de l'hélium. Nous avons ensuite obtenu des valeurs de $T_{\rm eff}$ et log g en utilisant les raies de Balmer. Ces données permettent de prédire le flux ultraviolet et, après les avoir normalisés à la magnitude Strömgren y, nous comparons ces spectres avec les observations. Nous trouvons un bon accord pour les objets avec $T_{\rm eff} <$ 31,000 K lorsqu'on tient compte de la présence d'éléments lourds et du rougissement interstellaire. Pour les étoiles avec $T_{\rm eff} >$ 31,000 K, nous remarquons une incohérence. Notamment, les raies prédites sont trop larges et le niveau du continu trop faible. Nous examinons les effets des éléments lourds sur les modèles d'atmosphères; pour des abondances solaires, l'effet est prononcé dans la région de l'ultraviolet lointain ce qui pourrait expliquer le désaccord observé.

Mots clefs:

étoiles: atmosphères, individuel (GD 323), naines blanches, paramètres fondamentaux, sous-naines — techniques: spectroscopique

Abstract

We present two spectroscopic studies of compact and evolved objects. Firstly, we report the discovery of spectroscopic variations in the DAB white dwarf GD 323. Using simultaneous optical spectroscopic observations of our target star and of a non-variable DA white dwarf, PG 1234+482, we find quasi-periodic variations in both hydrogen and helium features on a timescale of hours. The hydrogen lines vary in opposite phase from that of He I λ4471 and the amplitude variations of the equivalent width of Hβ are $\sim$ 30%. This result suggests an inhomogenous surface composition rather than a stratified atmosphere. We also investigate the consistency between atmospheric parameters derived from optical spectra of subdwarf B stars and the far-ultraviolet continuum flux. Optical and far-ultraviolet spectra were secured for a sample of nine sdB stars and pure hydrogen and mixed hydrogen-helium NLTE model atmosphere grids were computed. Using the Balmer line fitting technique, we derive values for $T_{\rm eff}$ and log g and use these to predict the ultraviolet flux which is then normalized at the observed Strömgren y magnitude. We find good agreement for stars with $T_{\rm eff} < 31{,}000$ K when some allowance is made for metal line blanketing and for the presence of small amounts of interstellar reddening. For objects with $T_{\rm eff} > 31{,}000$ K we find a systematic discrepancy: the predicted line profiles are too wide and the continuum flux level too low. We examine the effects of including line blanketing of heavy elements in solar abundances in our models and find significant effects in the far-ultraviolet range that could explain these inconsistent results.

Subject headings:

stars: atmospheres, fundamental parameters, individual (GD 323), subdwarfs, white dwarfs, — techniques: spectroscopic

Table des matières

Liste des figures

Liste des tableaux

Chapitre 1

Introduction

Lorsqu'une étoile termine sa vie relativement paisible sur la séquence principale, elle entame une série de phases évolutives, autant tranquilles que violentes, qui la mèneront à sa fin: celle d'un cadavre stellaire. En effet, après avoir épuisé son carburant nucléaire, l'étoile subit une succession d'expansions des couches externes et de contractions du coeur, et ce, jusqu'à ce qu'elle devienne instable. L'état final de l'étoile dépend en grande partie de sa masse initiale et, dans 90% des cas, l'évolution stellaire mène à une éjection de l'enveloppe externe, laissant ainsi un noyau central très compact et très chaud. Toute étoile ayant une masse inférieure à 8 $M_{\odot}$ termine sa vie de cette façon et devient une naine blanche. Ces objets sont caractérisés par des masses d'environ 0.6 $M_{\odot}$ et des rayons comparables à celui de la Terre. N'ayant plus de fusion nucléaire, elles se refroidissent avec le temps. De plus, elles sont composées d'un coeur de matière dégénérée entouré d'une mince enveloppe et résistent à l'effondrement gravitationnel grâce à la pression engendrée par un gaz d'électrons dégénérés.

Toutefois, il arrive que durant ce qu'on appelle le flash d'hélium, une phase qui déclenche de nouveau les réactions nucléaires après le premier épisode d'expansion/contraction, l'étoile perde une quantité substantielle de masse. Ce qui reste est un noyau d'hélium, très dense, qui continue de brûler, et qui est entouré d'une enveloppe d'hydrogène inerte et très mince (< 0.02 $M_{\odot}$). Ces étoiles sont des sous-naines et elles se situent sur la branche horizontale extrême du diagramme Hertzprung-Russell. Elles partagent plusieurs points en commun avec les naines blanches, telles leur masse (~ 0.55 $M_{\odot}$) et leur densité élevée, et aussi le fait qu'il s'agisse

d'objets dans un stade final de l'évolution stellaire. On croit que les sous-naines deviennent des naines blanches de faible masse lorsque leur carburant nucléaire est épuisé. En d'autres termes, les sous-naines sont les progéniteurs d'une fraction des naines blanches.

Les naines blanches et les sous-naines sont caractérisées par des propriétés atmosphériques (température effective, gravité de surface, et abondances chimiques) diverses. Dans le cas des naines blanches, la majorité d'entre elles sont classifiées DA, c'est-à-dire ayant des spectres qui ne montrent que des raies d'hydrogène. Cette pureté s'explique en partie par le phénomène de diffusion: le champ gravitationnel intense qui caractérise les naines blanches ($\log g \sim 8.0$) fait en sorte que les éléments lourds coulent vers le fond de l'atmosphère, tandis que les éléments plus légers remontent vers la surface. Cependant, on retrouve aussi des naines blanches qui possèdent des atmosphères riches en hélium. Cela signifie qu'il existe d'autres processus qui entrent en compétition avec le tri gravitationnel, telle la convection. Dans le cas des DB, des étoiles relativement froides ($T_{\rm eff} < 30,000$ K), ce sont des raies d'hélium neutre que l'on détecte, alors que les DO ($T_{\rm eff} > 45,000$ K) montrent des raies d'hélium ionisé (Wesemael et al. 1993).

Du côté des sous-naines, nous utilisons aussi une nomenclature spectrale. De façon générale, les sdB sont des étoiles ayant des spectres dominés par des raies de Balmer sur lesquelles se superposent de faibles raies d'hélium neutre, tandis que les sdOs, étant des étoiles plus chaudes, affichent des raies d'hélium ionisé. Par ailleurs, on remarque que la pureté chimique qui distingue les naines blanches est moins évidente dans les sous-naines, car les atmosphères de ces dernières contiennent des traces de plusieurs éléments lourds tels le fer et le carbone.

La spectroscopie est un outil indispensable dans l'analyse atmosphérique de ces deux classes d'étoiles puisqu'une foule d'informations peut être extraite de ces données. Nous présentons ici deux analyses spectroscopiques d'étoiles compactes et évoluées.

Dans le premier cas, nous nous penchons sur l'énigmatique naine blanche GD 323. Cette étoile est le prototype d'une classe particulière de naines blanches: les DAB. Ces étoiles, relativement rares, présentent à la fois des raies d'hydrogène et des raies d'hélium dans leur spectre. Toutefois, cette classe d'objets ne représente pas un groupe homogène. Dans certains cas, les observations s'expliquent par un système binaire non-résolu composé de deux naines

blanches – une de type DA et une de type DB. D'autres scénarios, impliquant par exemple l'accrétion, peuvent également expliquer la présence simultanée d'hydrogène et d'hélium. Par contre, GD 323 résiste toujours aux interprétations. Parmi les hypothèses proposées depuis sa découverte en 1984, aucune ne semble expliquer entièrement les observations. Jusqu'à récemment, le modèle le plus favorable était celui d'une atmosphère stratifiée où une couche d'hydrogène très mince 'flotte' sur une enveloppe d'hélium, nous permettant ainsi de détecter les deux éléments (Koester et al. 1994). D'autres modèles ont été proposés, entre autres celui d'une atmosphère homogène et aussi celui d'une atmosphère inhomogène. Par contre, aucun de ces modèles n'est adéquat, d'où l'importance de réétudier le problème.

Une question essentielle est celle de la variabilité spectroscopique. Si nous pouvions détecter des variations dans les largeurs équivalentes des raies, cela impliquerait qu'il y a des variations d'abondances chimiques à la surface de GD 323, favorisant ainsi le modèle d'une atmosphère inhomogène plutôt que stratifiée. Nous avons entrepris cette étude délicate, et avons essayé de détecter des variations soit sur une courte échelle de temps (quelques heures) ainsi que sur une échelle de temps plus longue (quelques jours). Nous présentons les résultats de cette analyse dans le chapitre 2.

Dans la deuxième étude, nous vérifions si les paramètres atmosphériques déterminés à partir de spectres visibles de sous-naines sont compatibles avec des données dans la région de l'ultraviolet lointain. Les paramètres atmosphériques nous donnent des informations importantes, qui nous aident ensuite à mieux comprendre les processus physiques qui ont lieu dans ces étoiles. Actuellement, plusieurs techniques existent qui nous permettent de déterminer ces paramètres. Une de ces techniques, utilisée de façon courante dans le domaine des naines blanches, est celle de l'analyse des raies de Balmer. Cette méthode s'applique également aux sous-naines, et nous permet ainsi d'estimer les valeurs de température effective et de gravité de surface.

En théorie, cette méthode pourrait également s'appliquer aux raies de Lyman dans l'ultraviolet. D'abord, ce genre d'analyse pourrait nous permettre d'avoir accès à une autre façon de déterminer les paramètres atmosphériques puisqu'il arrive parfois qu'on soit incapable de le faire en utilisant des spectres visibles. Ceci est le cas, par exemple, pour certains systèmes

binaires. De plus il serait possible de s'assurer qu'il existe une cohérence entre les paramètres obtenus à partir des raies de Lyman et à partir des raies de Balmer. Ce type d'étude est désormais possible grâce au satellite *FUSE* (*Far Ultraviolet Spectroscopic Explorer*) qui fut déployé en 1999, et qui nous permet de détecter les raies de Lyman à partir de Lyβ.

Une telle étude fut réalisée par Barstow et al. (2001, 2003) et Good et al. (2004) pour les naines blanches de type DA et DAO, respectivement. Dans ce cas, ils ont déterminé de façon indépendante les paramètres atmosphériques à partir de spectres *FUSE* et de spectres visibles. Leurs résultats montrent qu'il existe un bon accord pour des objets ayant des températures inférieures à $\sim$ 50,000 K. Une divergence apparaît pour les objets plus chauds.

Une analyse semblable peut également être complétée pour les sous-naines. Dans le chapitre 3, nous présentons une analyse d'un échantillon de neuf sous-naines de type spectral B.

Chapitre 2

Article

DISCOVERY OF SPECTROSCOPIC VARIATIONS IN THE DAB WHITE DWARF GD 323

C. Pereira, P. Bergeron, and F. Wesemael

Département de Physique, Université de Montréal, C.P. 6128, Succ. Centre-Ville, Montréal, Québec, Canada, H3C 3J7.

The Astrophysical Journal, 623: 1076-1082, 2005 April 20

Received 2004 December 9; accepted 2005 January 26

2.1 Abstract

We report the discovery of spectroscopic variations in GD 323, the prototypical DAB white dwarf. Simultaneous optical spectroscopic observations over five consecutive nights of GD 323 and of PG 1234+482, a non-variable comparison DA white dwarf of similar brightness, are used to reveal quasi-periodic variations in both the hydrogen and helium absorption lines over a timescale of hours. The amplitude of the variation of the equivalent width of Hβ is $\sim$ 30 %. Moreover, the strength of the hydrogen lines is shown to vary in opposite phase from that of He I λ4471. These results suggest that the model currently thought to be the most viable to account for the simultaneous presence of hydrogen and helium lines in GD 323, namely a static stratified atmosphere, may need to be reexamined. Instead, a model with an inhomogeneous surface composition, resulting perhaps from the dilution of a thin hydrogen atmosphere with the underlying helium convection zone, may be a better representation of GD 323. The observed variation timescale of $\sim$ 3.5 hours is consistent with the slow rotation rate of white dwarf stars.

2.2 Introduction

The DAB stars represent a class of white dwarfs with hybrid spectra, as weak neutral helium lines are superposed onto the classical hydrogen-line spectrum of DA stars (see, e.g., Wesemael et al. 1993). The prototype of this class, GD 323 (WD 1302 + 597; $V = 14.52$), was discovered independently by Oke et al. (1984) and Liebert et al. (1984). The latter made the first attempts at modeling the unusual hybrid spectrum of GD 323, and their results have since been updated and considerably upgraded by Koester et al. (1994) on the basis of a set of high-quality optical spectra of that star. Koester et al. (1994) were led to conclude that a stratified atmospheric structure, consisting of a thin ($\log M_{\rm H}/M_\star = -16.8$) hydrogen layer floating on top of a helium envelope, remained the "most promising" explanation of the bulk of the properties of GD 323.

Since this initial discovery, several additional stars spectroscopically classified as DAB stars have been unearthed: G104−27 (Holberg et al. 1990), HS 0209+0832 (Jordan et al.

1993), MCT 0128−3846 and MCT 0453−2933 (Wesemael et al. 1994), PG 1115+166 (Burleigh et al. 2001; Bergeron & Liebert 2002) and, most recently, PG 1603+432 (Vennes et al. 2004). The sample of DAB stars is quite inhomogeneous, however, as several distinct mechanisms have been called on to account for individual objects: thus, GD 323 could be a stratified object, while it has been argued in the discovery papers cited above that MCT 0128−3846, MCT 0453−2933, and PG 1115+166 are unresolved DA+DB binaries. This has now been confirmed for PG 1115+166 (Maxted et al. 2002) and MCT 0453−2933 (Napiwotzki & the SPY Consortium 2005). Furthermore, HS 0209+0832, while initially thought to be characterized by a homogeneous atmosphere (Heber et al. 1997a), now appears to be undergoing accretion (Wolff et al. 2000). The last object added to the list, PG 1603+432, seems characterized by a homogeneous composition.

Among those stars, the prototype GD 323 is perhaps the most thoroughly studied object. In their detailed analysis, Koester et al. (1994) investigate four distinct models: homogeneous and stratified composition, unresolved binary and spotted star. Despite this variety of options, they conclude that none of these models provides a completely satisfactory fit to the data, but that the stratified model is the most acceptable match. Given this ambiguous outcome, further investigations of these models appear in order.

An important ingredient in defining the correct model for GD 323 could be the question of variability. While the white light photometry of Robinson & Winget (1983) excludes photometric variations at the 0.25% level in the range 10–1200 s, it was suggested by Liebert et al. (1984) that the object be monitored for spectroscopic variations. This need became more acute with the report by Kidder et al. (1992) that the weak He I lines, initially observed by Holberg et al. (1990) in data at high S/N on the DAB star G104-27, were not seen in later spectra of comparable quality. A similar situation is encountered in HS 0209+0832, in which Heber et al. (1997a) report changes in the strength of the neutral and ionized helium lines over a one-year period. In GD 323, earlier spectra obtained by Liebert et al. (1984) and by J. L. Greenstein — initially displayed by Koester (1991a,b) and Wesemael et al. (1993) — unfortunately cannot provide any firm conclusion about the variability of that object, as these were obtained with different instrumental setups and spectroscopic resolutions.

To investigate whether GD 323 is a spectroscopic variable, Koester et al. (1994) obtained a series of nine high signal-to-noise ratio, ~ 7 Å resolution spectra of that object, all secured with an essentially identical instrumental setup. Six of these spectra were obtained within a single night, while the other three had been secured, respectively 15 days, 9 months, and one year earlier. On the basis of these spectra, the best and most homogeneous set secured at that time for a DAB star, Koester et al. (1994) concluded that the available data were compatible with the assumption that the star showed no variability. However, it was our feeling at the time that, while it was clear that there were no large-amplitude changes in the line spectrum of GD 323, the signal-to-noise ratio of the individual spectra was good enough to permit a much more detailed analysis of the variability of GD 323 than had been carried out by Koester et al. (1994). This was undertaken independently by Wesemael et al. (1995), but their analysis could not quite meet the burden of proof associated with an investigation of this type: while their results suggested the presence of small spectroscopic variations in the Koester et al. (1994) data, their analysis also showed that a well-planned observing strategy and a rigorous data reduction process would both be required in order to build a stronger case for the presence, or absence, of low-level spectroscopic variations in GD 323.

Recently, the opportunity arose to revisit the issue of spectroscopic variability of GD 323, and we succeeded in securing new data for that object that sheds some light on this 20 year-old problem. This paper summarizes the results of this revamped investigation.

2.3 Observations

2.3.1 Data Acquisition

As discussed above, the study of Koester et al. (1994) reveals that the spectroscopic variations in GD 323, if any, are quite small. Hence a careful observing strategy had to be developed to ensure that any variability detected in a series of time-resolved spectroscopic observations is intrinsic to the star and not the result of changes in the atmospheric transparency or of an artifice introduced in the data reduction. The best way to assess the variability of GD 323 is to secure in parallel spectroscopic observations of a constant comparison star. Ideally,

one would like to have both GD 323 and the comparison star on the slit in order to obtain simultaneous time-resolved spectroscopic observations. Unfortunately, no such star could be found in the vicinity of GD 323, and we had to rely on a different strategy.

We thus selected a comparison star based on the following set of criteria: firstly, we required a star with no known variations. We also required an object whose magnitude was similar to that of GD 323 ($V = 14.52$). Furthermore, we demanded that our comparison object have few spectral lines and a spectral energy distribution comparable to that of GD 323. Finally, we wanted an object that was as close as possible to our target object in the sky. Examination of the Catalog of Spectroscopically Identified White Dwarfs of Mccook & Sion (1999) revealed that the DA star PG 1234+482 was the most judicious choice. Past observations of PG 1234+482 have shown no evidence for variability, it has a visual magnitude of $V = 14.42$, and with an effective temperature of $T_{\rm eff} = 55,040$ K (Liebert et al. 2005, hereafter LBH), its spectrum consists of a well-defined continuum with only weak hydrogen lines. Finally, PG 1234+482 and GD 323 are separated by approximately 15 degrees on the sky.

Since we did not know *a priori* over what timescales variations might occur, we carried out spectroscopic observations over five consecutive nights, from 2004 February 10 to 14. Both GD 323 and PG 1234+482 were monitored for over 5 hours on the first night, and for about an hour on the remaining nights. These optical spectra were secured using the Steward Observatory 2.3 m reflector telescope equipped with the Boller & Chivens spectrograph and a Loral CCD detector. A 4.5 arcsec slit and a 600 line mm^{-1} grating in first order provided a spectral coverage of 3200-5300 Å at a resolution of $\sim$ 6 Å FWHM. Each 600 s spectroscopic observation of GD 323 was immediately followed by a 600 s exposure of PG 1234+482. The average signal-to-noise ratio per pixel and per exposure is $\sim$ 85 for GD 323 and $\sim$ 100 for PG 1234+482. In total, 27 spectra of GD 323 and 25 spectra of PG 1234+482 were secured, the vast majority of them under excellent observing conditions.

2.3.2 Data Reduction

The optical spectra were extracted and wavelength-calibrated using the Image Reduction and Analysis Facility (IRAF) standard package. A first cut at the flux calibration was obtai-

ned with IRAF using the various flux standards secured during the observing nights. However, in the course of our analysis, we realized that we could take advantage of our multiple spectroscopic observations of PG 1234+482, and use this star instead as a flux standard, at least in a relative sense. This method is analogous to that used for taking high-speed photometric observations of variable stars, where a constant comparison star is used to correct the light curve of the target star. The detailed procedure used in the reduction of our spectroscopic observations thus proceeded as follows.

The first step was to combine our 25 individual spectra of PG 1234+482, flux calibrated with IRAF as described above. This combined spectrum, characterized by a signal-to-noise ratio of ~ 340, was then fitted with a grid of synthetic white dwarf spectra, from which we derived $T_{\rm eff} = 54,200$ K and $\log g = 7.77$. This effective temperature is within 1.5 % from that derived by LBH on the basis of a lower signal-to-noise ratio spectrum. A synthetic spectrum calculated with these atmospheric parameters, which matches extremely well the combined observed spectrum, now serves as a noiseless template for the rest of the analysis. Flux calibration functions were then obtained by simply dividing this template by the individual unfluxed spectra of PG 1234+482 and smoothing the result with a 9-point filter. The application of these smoothed flux calibration functions to the unfluxed spectra of PG 1234+482 ensures that each resulting spectrum matches the synthetic template perfectly. The fluxed spectra for PG 1234+482 are shown in the right panel of Figure 2.1 for the first night, and in the right panel of Figure 2.2 for the remaining nights.

The next step was to use these derived functions to flux-calibrate the spectroscopic observations of GD 323. Specifically, we calibrate each spectrum of GD 323 with the function derived from the observation of PG 1234+482 that immediately follows. The resulting flux-calibrated spectra of GD 323 are displayed in the left panels of Figures 2.1 and 2.2. There are two main advantages to our approach: first we obtain flux calibrated spectra of our target star that are as independent as possible of the flux calibration provided by IRAF. Here, the IRAF package is used only to generate the average spectrum of PG 1234+482 used to define the noiseless synthetic template of that star. Once this template is defined, the uncoupling from IRAF in the procedure that generates calibrated spectra of GD 323 is complete (IRAF

spectra are used to generate our error estimate in § 3). This is a substantial advantage, given that the flux calibration is recognized to be the most delicate step of the reduction procedure. In addition, because of the nearly simultaneous observations of GD 323 and PG 1234+482, our method allows us to monitor small temporal changes in the atmospheric transparency.

As will be discussed further below, our conclusions about the variability of GD 323 do not hinge on the flux calibration procedure developed here, although the quality of the results has certainly benefited from this approach. One should also note that we did not worry about calibrating our spectra in terms of absolute fluxes, as we are mainly interested here in relative flux variations.

2.4 A Search for Spectroscopic Variations in GD 323

2.4.1 Single-Night Variations in Equivalent Widths

With our calibrated spectra in hand, we search for spectroscopic variations by measuring the equivalent widths of the most important hydrogen and helium absorption lines. The most delicate step in this procedure is to define the continuum in order to normalize the individual line profiles. A simple average over a few pixels on each side of the line is not accurate enough and can introduce undesirable uncertainties in the equivalent width measurements. We rely instead on a procedure similar to that outlined in LBH to define the location of the continuum in the far wings of the hydrogen Balmer lines.

We first construct a very high signal-to-noise template spectrum by combining our 27 spectroscopic observations of GD 323. This template spectrum displayed at the top of Figure 2.2 is then forced to match each single observation of GD 323 by multiplying the template by a polynomial of fifth degree in λ. The result of this procedure for a typical spectrum of GD 323 is illustrated in Figure 2.3. We define the continuum level over a given interval on the basis of the monochromatic flux in the template spectrum at the boundaries of the interval. We choose the following intervals over which the equivalent widths are to be measured: 4800-4925 Å, 4275-4425 Å, 4065-4150 Å, corresponding to Hβ, Hγ, and Hδ, respectively, as well as 4430-4510 Å and 4680-4750 Å for the He I λ4471 and He I λ4713 features, respectively. We

concentrate on these features since they are the strongest lines in the spectrum; other lines are visible, but are either weak or blended and can only be measured with difficulty. Furthermore, the wavelength intervals are chosen to include as much of the line wings as possible, while avoiding blending. The intervals over which the equivalent widths are measured are reproduced in Figure 2.3.

The equivalent width measurements as a function of time for the three hydrogen and the two neutral helium absorption lines in GD 323 are displayed in Figure 2.4 for the 14 spectra secured within the single night of 2004 February 10. These results show clearly that the hydrogen and He I λ4471 line strengths of GD 323 vary with time,and that these variations appear to be quasi-periodic. This was by no means expected, as we could very well have detected random variations, or no variations at all. Moreover, the observed variations occur on a relatively short timescale, with the feature strengths going from a maximum to a minimum over the course of a few hours only. Even more surprising, the variations of the hydrogen lines and λ4471 appear to be out of phase: as the hydrogen lines (especially Hβ and Hγ) get stronger, the helium line weakens and vice versa. The case for He I λ4713 is admittedly much weaker and we cannot, at this stage, account completely for its behavior: while the line is reasonably strong and unaffected by blending, the variations it displays appear more muted than those observed in λ4471, and their phasing with the hydrogen lines much less obvious.

2.4.2 Error Analysis

A preliminary estimate of the errors in the equivalent width measurements for the three hydrogen lines in GD 323 has been obtained from a consideration of the spectrum of the comparison star PG 1234+482. We have measured the equivalent widths for each line on the 13 individual fluxed spectra of that star secured on 2004 February 10. The rms error on the equivalent widths reflects the S/N ratio of the individual spectra and the reliability of the procedure used to set the continuum level (§ 2). They amount to 0.03 Å for Hβ, 0.08 Å for Hγ, and 0.03 Å for Hδ. These errors can be considered as lower limits, as the use of smoothed flux calibration functions applied to the raw individual spectra of PG 1234+482 guarantees a perfect match of the continuum flux in individual spectra with the template of that star. When

the same smoothed flux calibration functions are applied to the raw individual spectra of GD 323, the match to the average, or template, spectrum of GD 323 is not as good, since residual calibration errors remain. It is not possible to evaluate these calibration errors, however, as they cannot be disentangled from the intrinsic variations of GD 323.

To estimate these residual calibration errors, we have opted to go back to the 13 individual IRAF-reduced spectra of PG 1234+482 acquired on 2004 February 10. Because these spectra were simply reduced with the standard IRAF package, the rms deviations over a single night are deemed to include contributions from the S/N ratio of the individual spectra, from the continuum setting and, more importantly, from any residual calibration error associated with IRAF. While our standard reduction is decoupled from IRAF (§ 2.2), it is our feeling that the rms errors generated in this way are more representative of the true uncertainties associated with our procedure. Their values are: 0.27 Å for Hβ, and 0.16 Å for Hγ and Hδ.

These IRAF-based error bars are included in Figure 2.4. For the neutral helium lines λ4471 and λ4713, both absent in the spectrum of PG 1234+482, we also measure the rms errors for Hϵ (0.20 Å), the Balmer line that is closest in average equivalent width to the two weaker He I lines.

2.4.3 Single-Night Variations in Calibrated Spectra

An alternative way of illustrating these variations is to divide the template spectrum of GD 323 (shown in Fig. 3) by each observed spectrum. Were GD 323 a constant star, this procedure should yield a straight line with random noise. The results for 3 spectra obtained on 2004 February 10 are displayed in Figure 2.5 at carefully selected phases. The bottom spectrum corresponds to a phase where the hydrogen line equivalent widths go through a minimum in Figure 2.4, while the top one corresponds to a maximum, and the middle spectrum is for an intermediate value; the trend is in the opposite direction for the helium lines. Also shown are the wavelength intervals used to measure the equivalent widths. Our results indicate that the flux variations never exceed 5 % throughout the spectrum. A close examination reveals, however, that in the case of the 1043 spectrum, there is less flux in the hydrogen features and more flux in the He I features, while the opposite is true for the 1226 spectrum, even when

taking into account the noise level. By integrating these small variations over the entire line profiles, we reduce the effect of the noise, and increase the significance of these variations. Indeed, even a 1% flux variation over a 100 Å wide Hβ line profile yields a 1 Å equivalent width variation, which is roughly the size of the variations observed in Figure 2.4.

2.4.4 Single-Night Variations in IRAF-calibrated and Uncalibrated Spectra

To reinforce these conclusions, we have carried out in parallel an analysis of the spectroscopic observations of GD 323 and PG 1234+482, but this time on data that were flux calibrated with IRAF. An additional analysis was also carried out directly with the unfluxed spectra. In both cases, the quasi-periodic variations in the hydrogen and helium features uncovered in § 3.1 could also be detected, although the quality of the results was significantly reduced. The fact that we were able to achieve similar results via several methods makes it unlikely that the variations uncovered in this paper are due to some artifice in the data acquisition or reduction procedures.

2.4.5 Variations over longer timescales

The equivalent width measurements for all five successive nights — a total of 27 observations — are shown in Figure 2.6 for the aforementioned features. The variations observed on the first night persist on the following nights, although only a segment of the quasi-sinusoidal variations is observed. Remarkably, on a given night, all hydrogen lines follow a similar pattern of variations, while the helium lines also share a common pattern, different from that of the hydrogen lines. Our attempts to fit a single periodic function through all the data points have failed, indicating that the variations are only quasi-periodic.

2.5 Discussion

The spectroscopic variations uncovered in GD 323 occur on timescales of the order of 3.5 h. Were these variations associated with the rotation of the underlying white dwarf ($R = 1.4 \times 10^{-2}\,R_{\odot}$), they would correspond to an equatorial velocity $v = 5\,\mathrm{km\,s^{-1}}$. This number is quite in line with the idea that most white dwarfs of both DA and DB types are very slow

rotators (Heber et al. 1997b; Koester et al. 1998; Dufour et al. 2002; Karl et al. 2005). This suggests that the association of the 3.5 h timescale with stellar rotation is reasonable.

It is also possible to revisit the issue of secular spectroscopic variations on timescales of years in the spectrum of GD 323. The first digital optical spectra of GD 323 were obtained over 20 years ago, but the different instrumental setups and resolutions used always hampered a direct comparison with spectra secured more recently (Liebert et al. 1984; Koester et al. 1994). However, the setup for the observations of Koester et al. (1994) and ours is quite similar and this provides a better basis for the comparison of high S/N ratio spectra secured 11 years apart. A comparison of the average spectrum of Koester et al. (1994) for the night of 1993 March 31 (average of 6 spectra) with our so-called template spectrum (average of 27 spectra) is shown in Figure 2.7. Although the reduction procedures differ, the claim can certainly be made that there are no large-amplitude secular variations in the spectrum of GD 323 over that baseline. However, small variations, most notably in He I λ4026 and He I λ4471, may be present.

The detection of spectroscopic variations on a 3.5 h timescale in GD 323 forces us to revise our ideas about this unusual object. As discussed in the Introduction, the thorough analysis of Koester et al. (1994) suggested that none of the options they considered provided a completely satisfactory fit to the data, but the stratified model provided the most acceptable match to GD 323. It seems difficult to understand now how the spectroscopic variations uncovered here could be accommodated by a static, layered model or, for that matter, by a static homogeneous hydrogen-rich atmosphere containing traces of helium.

Our findings suggest instead that an inhomogeneous surface abundance distribution in a slowly rotating star should be favored. Models with inhomogeneous surface abundances were discussed by Beauchamp et al. (1993), who considered several belt and cap geometries, and by Koester et al. (1994), who considered a spot model. Can such models reproduce the basic characteristics of GD 323 ? Let us consider the conclusions of Koester et al. (1994) first: they model the spot geometry by adding appropriately weighted fluxes from model atmospheres of DA and DB stars and restrict, on physical grounds, the difference in effective temperatures of these models to less than 5000 K. The conclusion they derive from the analysis of spotted

models is a familiar one (see, e.g., Liebert et al. 1984); namely that it is difficult to find a single model (characterized here by the effective temperature of the hydrogen-rich and helium-rich spots and by the relative surface they cover) that matches both the hydrogen and helium line strength and the slope of the energy distribution of GD 323.

In an earlier analysis, Beauchamp et al. (1993) had used more sophisticated models that considered specific geometries (equatorial belts and polar caps) and included a self-consistent treatment of the limb darkening effects. Sample optical spectra of models with a pure helium equatorial band and pure hydrogen polar caps from that investigation are reproduced here in Figure 2.8 and contrasted with our average spectrum of GD 323. These results illustrate how the strength of the hydrogen and helium lines, and in particular their relative strength, depends on both the extent of the helium-rich belt and on the inclination of the stellar symmetry axis with respect to the line of sight (given here by the angle $\theta_{\rm axis}$). For a given half-width of the pure helium equatorial band of $\Delta\alpha = 45°$, the hydrogen lines are stronger and the helium lines weaker when the star is seen pole-on ($\theta_{\rm axis} = 0°$) instead of equator-on ($\theta_{\rm axis} = 90°$). Similarly, for a given inclination axis of $\theta_{\rm axis} = 0°$ (pole-on), the helium lines become stronger and the hydrogen lines weaker when the half-width of the pure helium equatorial band is increased from $\Delta\alpha = 45°$ to 60°. In the present context, variations of the hydrogen and helium line strengths in opposite phase could be reproduced if the rotation axis and the symmetry axis are misaligned. While no optimal fit is provided here or in the investigation of Beauchamp et al. (1993), the results of Beauchamp et al. appear more encouraging than those of Koester et al. (1994). In particular, they encountered no major difficulty in matching the energy distribution with a model that gave an acceptable, although admittedly far from perfect, fit to the average optical spectrum of GD 323.

The modeling of surface inhomogeneities in terms of spots, or caps and belts, can perhaps lead one to believe that the origin of these surface features must be directly related to the presence of a magnetic field at the stellar surface. In that picture, GD 323 would be a low-field analog of Feige 7, a DAB white dwarf with a 35 MG dipolar field (Achilleos et al. 1992). In GD 323, the null circular polarization measurement of Angel et al. (1981) yields a 3σ upper limit of 3 MG on the longitudinal field component at the stellar surface. However, the idea that

surface inhomogeneities are related to other processes, such as the convective dilution of a thin overlying hydrogen envelope, should also be entertained. Indeed, it has been pointed out a while back (Liebert et al. 1987) that GD 323 is slightly cooler than the red edge of the DB gap, that peculiar region between 45,000 K and 30,000 K that appears to be devoid of helium-atmosphere degenerates. Models of the spectral evolution of white dwarfs (e.g., Fontaine & Wesemael 1987) attempt to account for this gap by calling on the dilution of a thin hydrogen layer at the surface of a 30,000 K DA star with the more massive helium envelope, dilution that would lead to a DA→DB transition near that effective temperature. If GD 323 were understood in those terms, an idea that we favor, its surface might be characterized by the presence of horizontal abundance gradients. Unfortunately, it is not possible to be more specific since a complete picture of the mixing process still eludes us at this stage. The geometries considered in the exploratory investigations of Beauchamp et al. (1993) and Koester et al. (1994) appear reasonable starting points for a renewed and more thorough study of that possibility.

We thank the director and staff of the Steward Observatory for the use of their facilities, and A. Beauchamp for his essential contribution to the calculation of models with surface inhomogeneities. This work was supported in part by the NSERC Canada and by the Fund FQRNT (Québec).

2.6 References

Achilleos, N., Wickramasinghe, D. T., Liebert, J., Saffer, R. A., & Grauer, A. D. 1992, ApJ, 396, 273

Angel, J. R. P., Borra, E. F., & Landstreet, J. D. 1981, ApJS, 45, 457

Beauchamp, A., Wesemael, F., Fontaine, G., & Bergeron, P. 1993, in White Dwarfs: Advances in Observation and Theory, ed. M. A. Barstow, NATO ASI Series, vol. 403, 281

Bergeron, P., & Liebert, J. 2002, ApJ, 566, 1091

Burleigh, M., Bannister, N., & Barstow, M. 2001, in ASP Conf. Ser. 226, 12th European Workshop on White Dwarf Stars, ed. J. L. Provencal, H. L. Shipman, J. MacDonald, & S. Goodchild (San Francisco: ASP), 135

Dufour, P., Wesemael, F., & Bergeron, P. 2002, ApJ, 575, 1025

Fontaine, G., & Wesemael, F. 1987, in I.A.U. Colloquium 95, The Second Conference on Faint Blue Stars, ed. A.G.D. Philip, D.S. Hayes, & J. Liebert (Schenectady: L. Davis Press), 319

Heber, U., Napiwotzki, R., Lemke, M., & Edelmann, H. 1997a, A&A, 324, L53

Heber, U., Napiwotzki, R., & Reid, I. N. 1997b, A&A, 323, 819

Holberg, J. B., Kidder, K. M., & Wesemael, F. 1990, ApJ, 365, L77

Jordan, S., Heber, U., Engels, D., & Koester, D. 1993, A&A, 273, L27

Karl, C., Napiwotzki, R., Heber, U., Dreizler, S., Koester, D., & Reid, I. N. 2004, A&A, in press

Kidder, K. M., Holberg, J. B., Barstow, M. A., Tweedy, R. W., & Wesemael, F. 1992, ApJ, 394, 288

Koester, D. 1991a, in Evolution of Stars: The Photospheric Abundance Connection, ed. G. Michaud & A. Tutukov, (Dordrecht: Kluwer), 435

Koester, D. 1991b, in White Dwarfs, ed. G. Vauclair & E.M. Sion, NATO ASI Series, Series C, no. 336 (Dordrecht: Kluwer), 343

Koester, D., Dreizler, S., Weidemann, V., & Allard, N. F. 1998, A&A, 338, 612

Koester, D., Liebert, J., & Saffer, R. A. 1994, ApJ, 422, 783

Liebert, J., Bergeron, P., & Holberg, J. B. 2005, ApJS, 156, 47 (LBH)

Liebert, J., Fontaine, G., & Wesemael, F. 1987, Mem. Soc. Astr. Italiana, 58, 17

Liebert, J., Wesemael, F., Sion, E. M., & Wegner, G. 1984, ApJ, 277, 692

Maxted, P. F. L., Burleigh, M. R., Marsh, T. R., & Bannister, N. P. 2002, MNRAS, 334, 833

McCook, G. P., & Sion, E. M. 1999, ApJS, 121, 1

Napiwotzki, R. and the SPY Consortium 2005, in ASP Conf. Ser., 14th European Workshop on White Dwarfs, ed. D. Koester & S. Moehler, in press

Oke, J. B., Weidemann, V., & Koester, D. 1984, ApJ, 281, 276

Robinson, E. L., & Winget, D. E. 1983, PASP, 95, 386

Vennes, S., Dupuis, J., & Chayer, P. 2004, ApJ, 611, 1091

Wesemael, F., Bergeron, P., & Briand, E. 1995, JRASC, 89, 183

Wesemael, F., Bergeron, P., Lamontagne, R., Fontaine, G., Beauchamp, A., Demers, S., Irwin, M. J., Holberg, J. B., Kepler, S. O., & Vennes, S. 1994, ApJ, 429, 369

Wesemael, F., Greenstein, J. L., Liebert, J., Lamontagne, R., Fontaine, G., Bergeron, P., & Glaspey, J. W. 1993, PASP, 105, 761

Wolff, B., Jordan, S., Koester, D., & Reimers, D. 2000, A&A, 361, 629

2.7 Figures

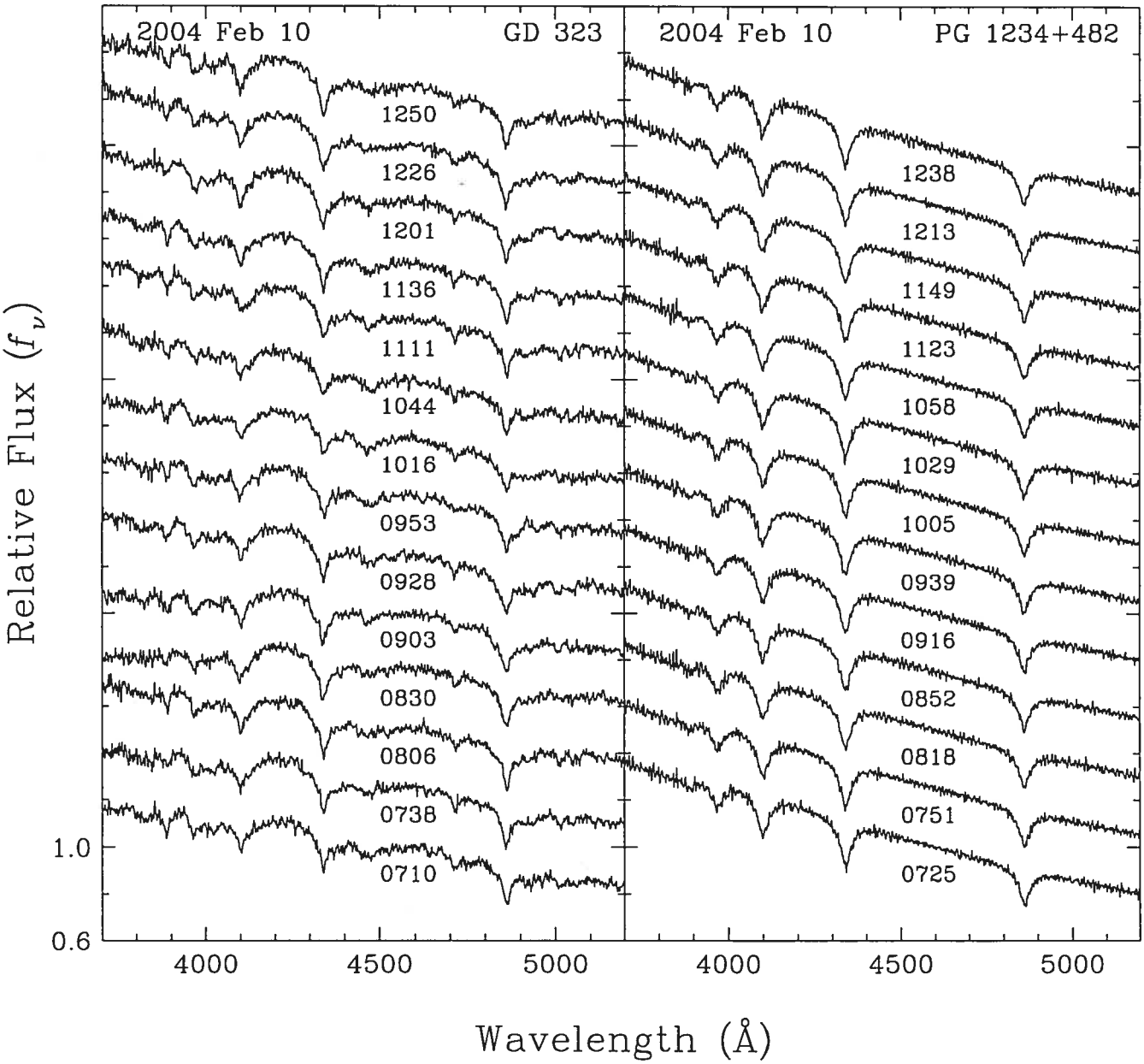

FIGURE 2.1 – Optical spectra of GD 323 (*left panel*) and PG 1234+482 (*right panel*) taken on 2004 February 10. The spectra appear in chronological order from the bottom up and are labeled with the corresponding universal time at which the integration was started. The spectra have been flux calibrated, normalized to unity at 4600 Å and offset from each other by a factor of 0.25 for clarity.

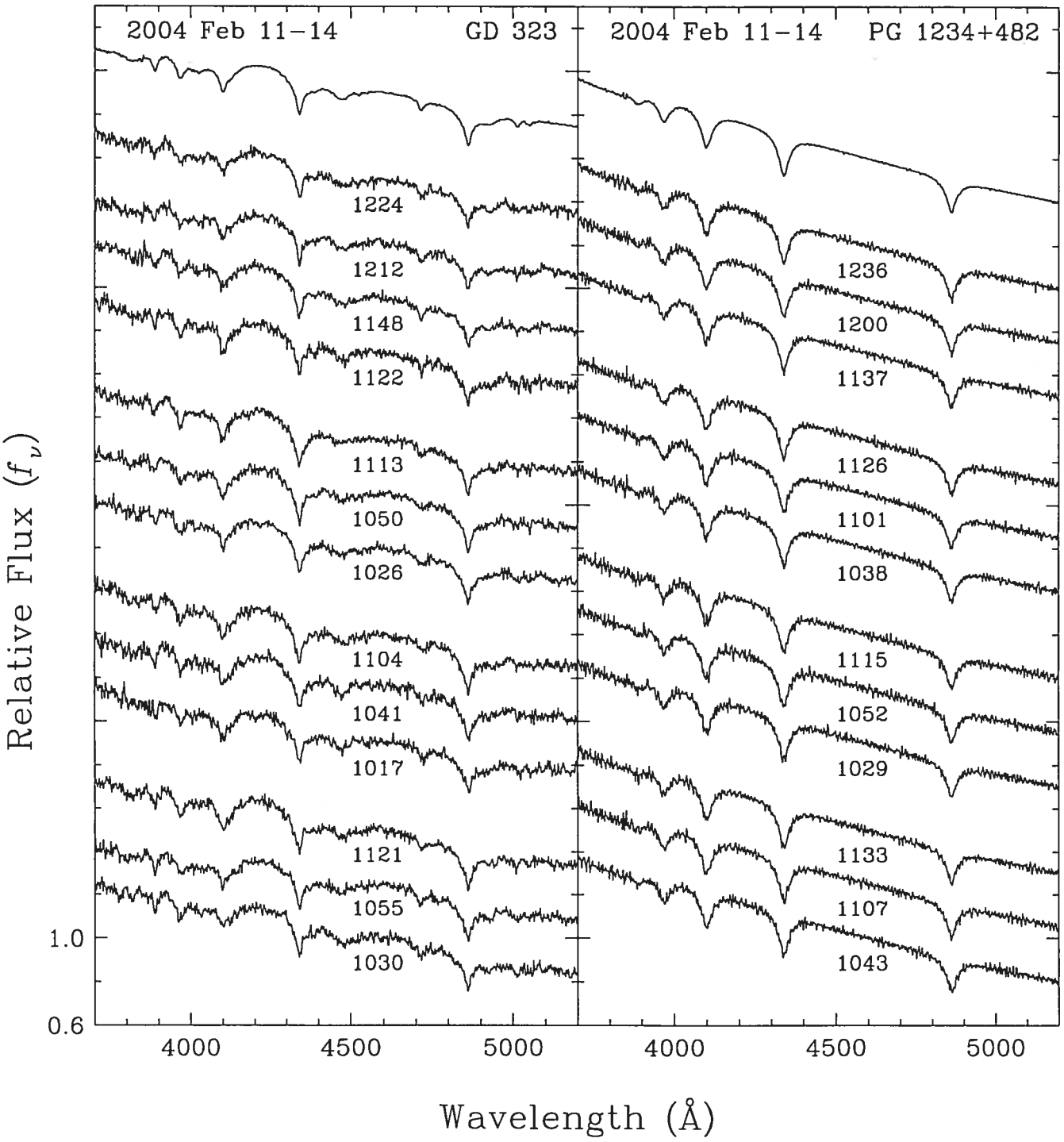

FIGURE 2.2 – Optical spectra of GD 323 (*left panel*) and PG 1234+482 (*right panel*) taken on 2004 February 11-14. The spectra appear in chronological order from the bottom up and are labeled with the corresponding universal time at which the integration was started. The spectra have been flux calibrated, normalized to unity at 4600 Å and offset from each other by a factor of 0.25 within the same night and by 0.3 between consecutive nights. The combined spectrum of GD 323 from all nights is also displayed at the top of the left panel; for comparison, the combined spectrum of PG 1234+482 is displayed at the top of the right panel.

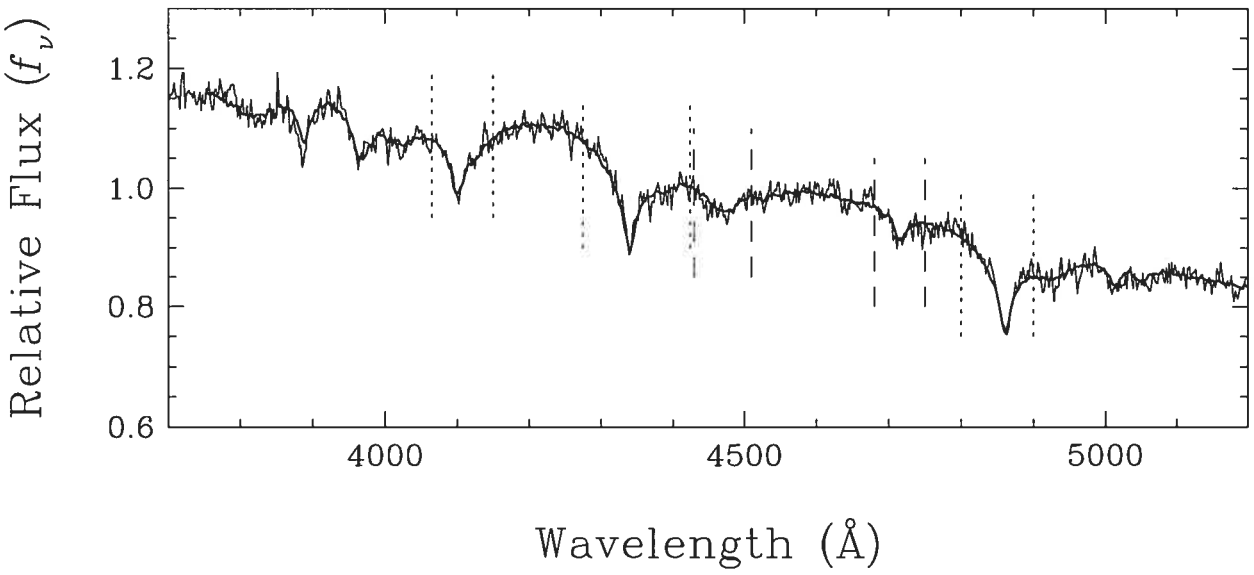

FIGURE 2.3 – Template spectrum (average of 27 spectra) superimposed on a typical spectrum of GD 323. Here, the template continuum has been adjusted to that of the observed spectrum using the procedure described in the text. This is done for each individual spectrum. The wavelength range used to measure the equivalent widths is shown for the hydrogen (*dotted lines*) and the He I (*dashed lines*) absorption lines.

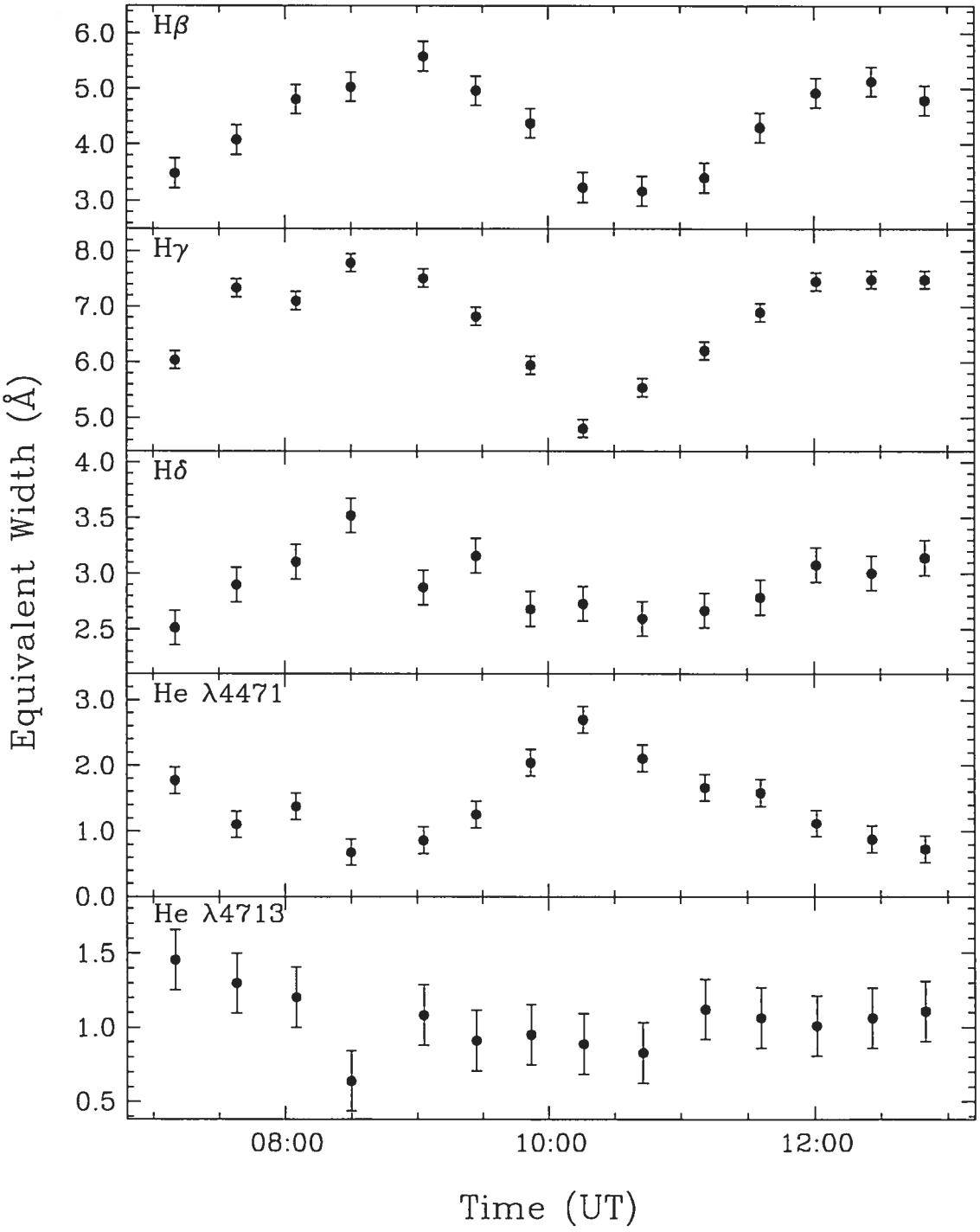

FIGURE 2.4 – Equivalent widths as a function of time (hours UT) for the spectra of GD 323 taken on 2004 February 10. The panels correspond to Hβ, Hγ, Hδ, He I λ4471 and He I λ4713 from top to bottom. The error bars are estimated from the equivalent width measurements of PG 1234+482, which showed no significant variations and had a similar signal-to-noise ratio. These values are then used as error bars for GD 323.

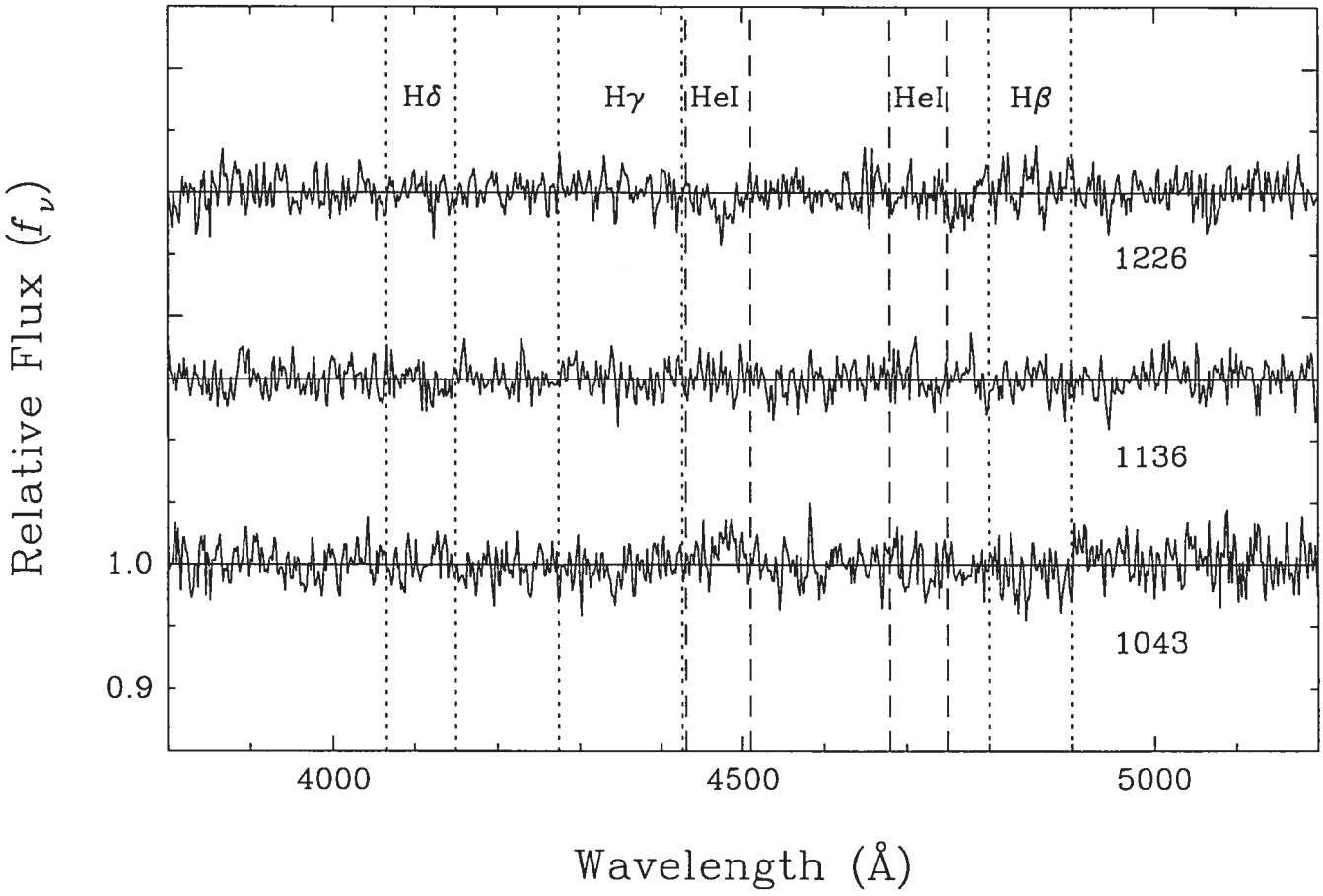

FIGURE 2.5 – Results obtained by dividing the fitted template spectrum of GD 323 (see, e.g., Fig. 2.3) by the observed spectra. The spectra are all taken on 2004 February 10, and they are labeled with the universal time of their acquisition. The spectra selected correspond to various phases where the hydrogen line strengths go from a minimum to a maximum, from bottom to top. The wavelength range used for the equivalent width measurements are indicated for the five strong features:Hβ-Hδ (*dotted lines*), He I λ4471 and He I λ4713 (*dashed lines*).

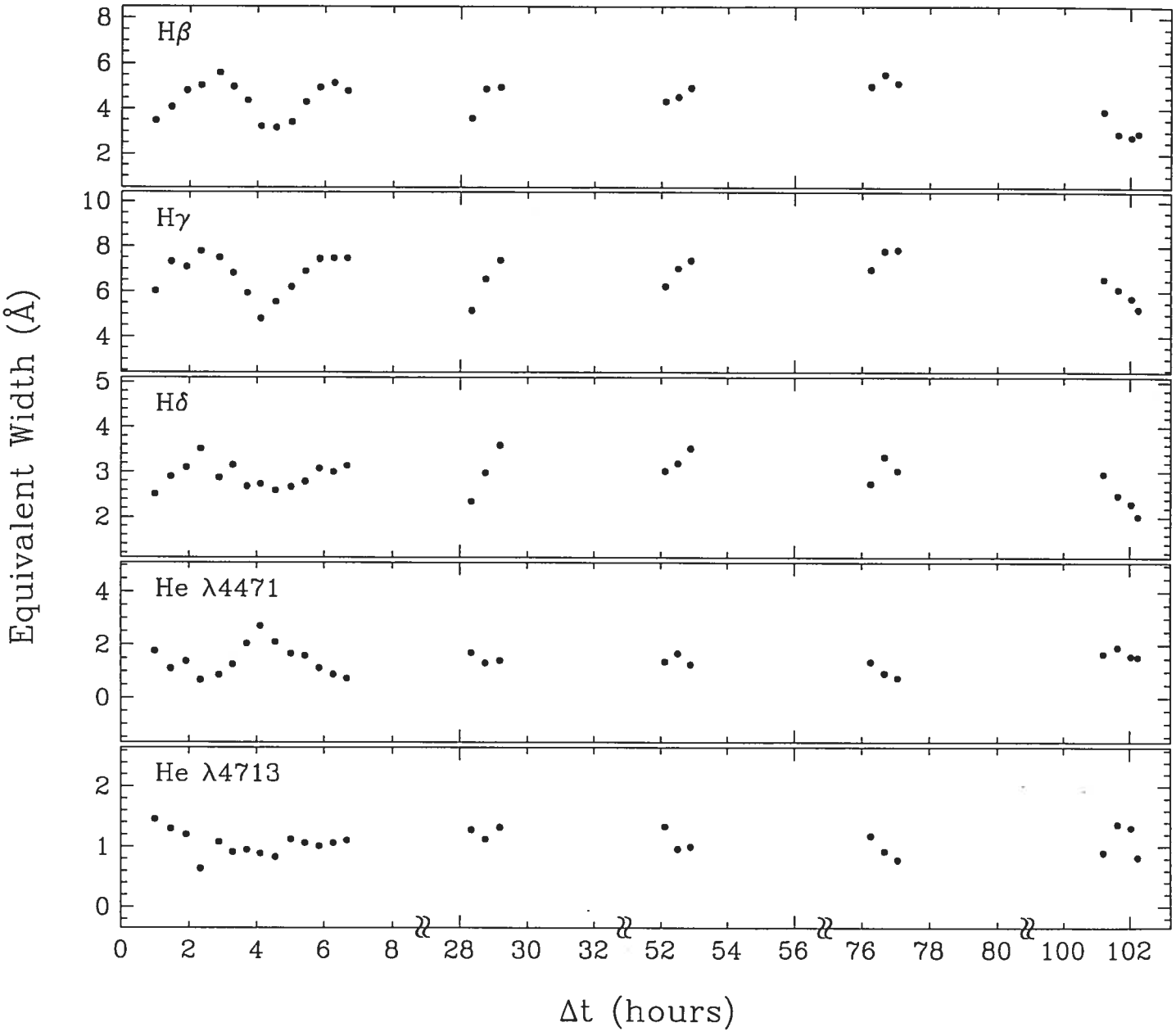

FIGURE 2.6 – Equivalent widths as a function of relative time (in hours) for the spectra of GD 323 taken over five nights, namely from 2004 February 10-14. The first observation is offset from $t = 0$ by one hour. The panels correspond to Hβ, Hγ, Hδ, He I λ4471 and He I λ4713 from top to bottom. The error bars are the same as those shown in Figure 2.5 but are omitted for clarity.

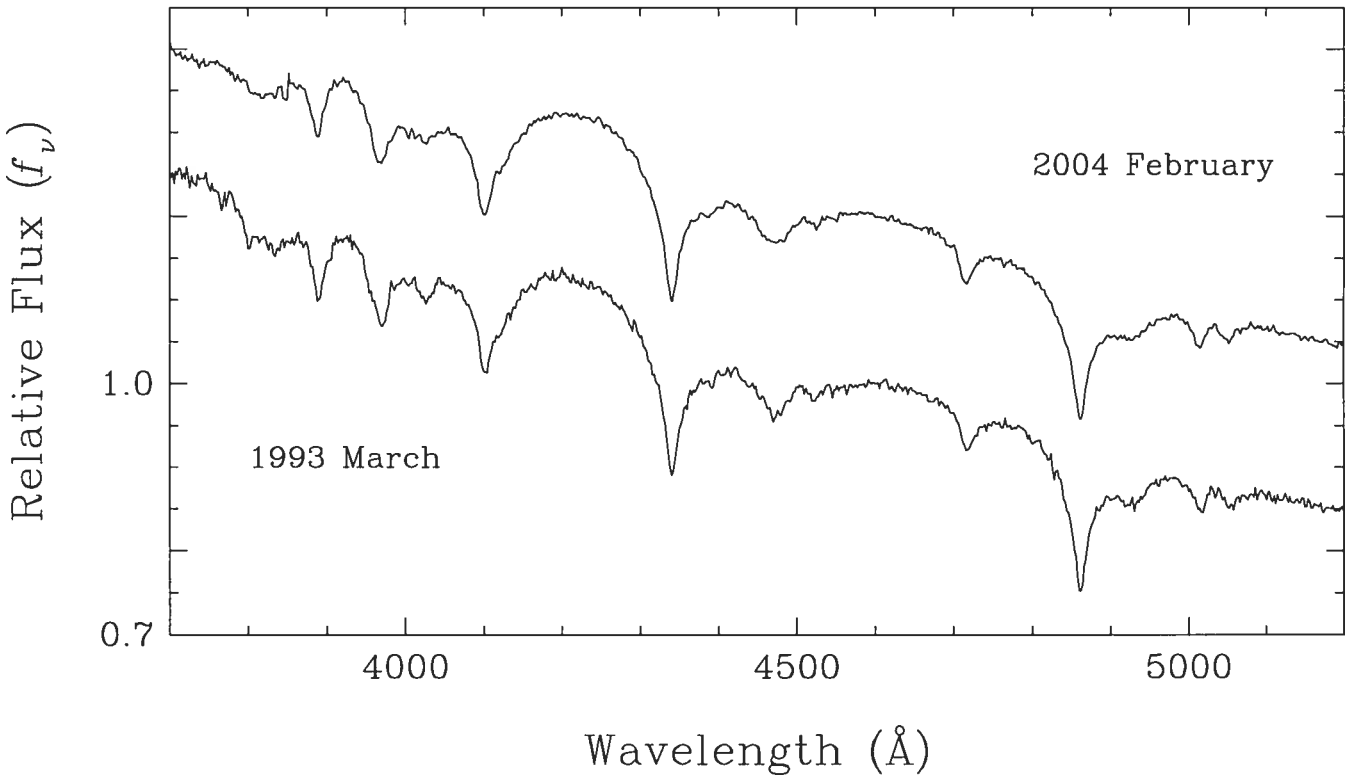

FIGURE 2.7 – Comparison of our template spectrum of GD 323 (average of 27 spectra) with that generated from the data of Koester et al. (1994) for the night of 1993 March 31 (average of 6 spectra). The spectra are normalized to unity at 4600 Å and offset from each other by a factor of 0.2. The instrumental setup was similar between the two sets of observations, but the reduction procedure was different (see text).

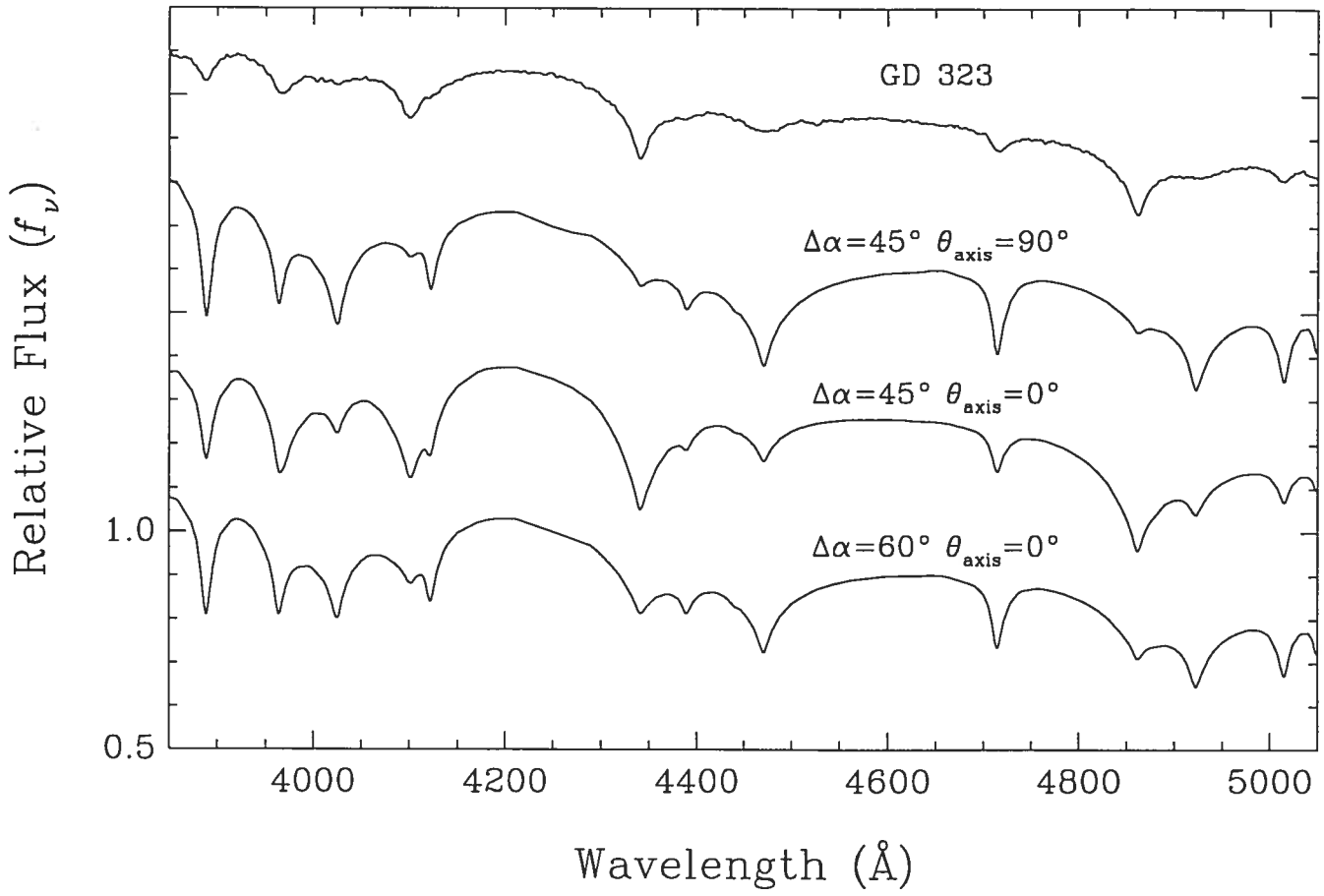

FIGURE 2.8 – Sample optical spectra of models with a pure helium equatorial band and pure hydrogen polar caps; the top spectrum is that of GD 323 (average of 27 observations) The spectra are normalized to unity at 4250 Å and offset from each other by a factor of 0.35. The half-width of the pure helium equatorial band is given by $\Delta\alpha$, while $\theta_{\rm axis}$ represents the angle between the stellar symmetry axis and the line of sight.

Chapitre **3**

Article

A CONSISTENCY CHECK BETWEEN THE BALMER LINES AND THE FAR-ULTRAVIOLET SPECTRUM IN SUBDWARF B STARS

C. Pereira, F. Wesemael, and P. Bergeron

Département de Physique, Université de Montréal, C.P. 6128, Succ. Centre-Ville, Montréal, Québec, Canada, H3C 3J7.

To be submitted to: The Astrophysical Journal

3.1 Abstract

We investigate the consistency between atmospheric parameters of subdwarf B stars derived from optical spectra and the far-ultraviolet continuum flux. Optical spectra were secured for a sample of nine sdB stars whose far-ultraviolet spectra were obtained from the *Far-Ultraviolet Spectroscopic Explorer (FUSE)* satellite archives. We compute pure hydrogen and mixed hydrogen-helium NLTE model atmosphere grids along with synthetic spectra. Applying the Balmer line fitting technique, we derive values for $T_{\rm eff}$ and $\log g$ for our sample objects, and these are then used to predict the far ultraviolet continuum flux. To do this, we normalize the predicted ultraviolet fluxes to the observed Strömgren y magnitude. Overall, we find satisfactory agreement for objects with $T_{\rm eff} < 31,000$ K, in the sense that the line profiles and continuum are well reproduced, when some allowance is made for the presence of line blocking from heavy elements or for the presence of small amounts of interstellar reddening, or both. For sdB stars with $T_{\rm eff} > 31,000$ K, we find a systematic discrepancy in the sense that the predicted line profiles are too wide, while the continuum levels are too low. We examine the effects of including line blanketing by heavy elements in solar abundances in our model calculations. Our preliminary results show that the blanketing effect in the ultraviolet is large, and could explain the inconsistent results obtained above $T_{\rm eff} = 31,000$ K.

3.2 Introduction

The field subdwarf B stars are the analog of the evolved, subluminous stars found on the extended horizontal branch (EHB) in globular clusters. They are low mass objects ($\sim 0.55\ M_{\odot}$) with helium burning cores and very thin hydrogen envelopes ($< 0.02\ M_{\odot}$) that are practically inert. Their evolution is not fully understood yet, although several formation channels have been proposed. Current scenarios include binary white dwarf mergers (Iben & Tutukov 1986), and the substantial mass loss of red giants either through stellar winds (D'Cruz et al. 1996) or through helium mixing (Sweigart 1997). In these three cases the result is a single sdB star. However, because more than two thirds of subdwarfs are in binary systems (Maxted et al. 2001), alternative formation scenarios are needed for this channel; these have been discussed

by Han et al. (2002, 2003). Moreover, B subdwarfs are thought to evolve into white dwarf stars, although only a small percentage of white dwarfs are formed this way (Saffer et al. 1994).

Spectroscopically, the B subdwarfs show spectra dominated by broad Balmer lines and weak He I lines and have effective temperatures between 20,000 K and 35,000 K. Helium has long been known to be deficient (see, for example, Edelmann et al. 2003), while the photospheric abundances of heavy elements display complicated patterns. Depending on the element, the abundance can be either under- or overabundant with respect to the solar value. Several physical processes such as gravitational settling, radiative levitation, and stellar winds are thought to play a role in determining the resulting abundance, but the details are not yet understood (see, for example, Bergeron et al. 1988; Michaud et al. 1988; Fontaine & Chayer 1997; Unglaub & Bues 2001)

In order to determine the relative importance of the processes at play in the photospheres of sdB stars, the basic atmospheric parameters of any given star must first be determined. Initially, optical photometry and ultraviolet energy distributions were used to determine the effective temperature, while the profiles of a handful of Balmer lines were used to derive the surface gravity (see e.g., Heber et al. 1984, 1986; Moehler et al. 1990; Wesemael et al. 1997). More recently, under the impetus of Saffer et al. (1994), the Balmer line fitting technique used in white dwarf work was adapted to the sdB stars. Here, the observed Balmer lines extending well into the blue are simultaneously fit using synthetic spectra generated from model atmospheres as well as a chi-squared minimization technique. This technique provides reliable estimates of the effective temperature, surface gravity and photospheric abundance (see, e.g. Saffer et al. 1994). With the advent of instruments such as *FUSE*, whose spectral coverage includes the Lyman line series from Lyβ onwards, one could in principle apply the fitting technique to this wavelength region. By doing so, one could check the consistency between the two sets of derived parameters.

This consistency has already been explored for DA white dwarfs by Barstow et al. (2001, 2003) and for DAO white dwarfs by Good et al. (2004). Their endeavour was motivated by the difficulty encountered in determining white dwarf parameters of binary systems. In

such cases, if the companion is more luminous, it is this star's spectrum that dominates in the optical region. However, in the ultraviolet region, it is the flux from the degenerate star that dominates, thereby providing access to atmospheric parameter determination. Barstow et al. (2001, 2003) found that, for DA white dwarfs, there was a good agreement between the two methods for temperatures up to $\sim 50,000$ K. At higher temperatures discrepancies were found, whereby Lyman line values were systematically higher. There, unresolved calibration issues, neglected trace abundances of selected heavy elements, and uncertainties in the physics included in the atmosphere models are all possible contributors to the observed discrepancy (Barstow et al. 2003; Vennes et al. 2005).

Motivated by these studies, we report here preliminary results of a similar analysis carried out for subdwarf B stars. For this purpose, we concentrated on a sample of nine subdwarf B stars for which we secured both optical and far-ultraviolet spectra. In § 2, we present both optical and far-ultraviolet spectroscopy, while in § 3, we discuss the grids of model atmospheres calculated for this investigation. The importance of NLTE effects and of heavy elements for these models are then discussed in § 4. The fits to the Balmer lines are presented in § 5, and the issue of the Lyman lines is discussed in § 6. Our main conclusions are then summarized in § 7.

3.3 Observations

3.3.1 Optical Spectra

A sample of nine subdwarf B stars was selected for this analysis. The candidates were chosen in order to provide objects covering a fair range of effective temperatures and surface gravities, as well as various helium and heavy element abundances. In practice, the sample includes cool sdB stars such as HD 4539 ($T_{\rm eff} \sim 24,000$ K, $\log g \sim 5.2$) as well as hotter objects like Ton S$-$227 ($T_{\rm eff} \sim 34,500$ K, $\log g \sim 6.0$). Table 1 lists the objects in our sample in order of increasing temperature along with alternative names. The Strömgren y magnitude is also provided, together with its reference. Optical spectra at high signal-to-noise ratio were secured with the 2.3 m reflector telescope at Steward Observatory in November 2004. The telescope

was equipped with the Boller & Chivens spectrograph and a Loral CCD detector. A 4.5 arcsec slit and a 600 line mm^{-1} grating in first order provided a spectral coverage of 3200-5300 Å at a resolution of $\sim$ 6 Å FWHM. The optical spectra were extracted, wavelength and flux-calibrated using the Image Reduction and Analysis Facility (IRAF) standard package. These are shown in Figure 3.1 and appear in order of decreasing temperature from top to bottom. The spectra are normalized to unity at 4600 Å and are offset from each other by a factor of 0.6 for clarity. Besides the strong Balmer lines from Hβ onwards, the spectra sometime show a weak He I λ4471.

3.3.2 Far-Ultraviolet Spectra

The far-ultraviolet spectra were obtained from the *Far Ultraviolet Spectroscopic Explorer* (*FUSE*) satellite archives. Moos (2000) provides an overview of the mission, while Sahnow (2000) describes the on-orbit performance of the satellite. The instrument aboard *FUSE*, launched in 1999, consists of four co-aligned channels. Each is comprised of a mirror, a focal plane assembly, a diffraction grating and two detectors. Two of the mirrors and gratings are coated with SiC thereby providing sensitivity to wavelengths below 1020 Å, while the other two mirrors and gratings are coated with LiF on Al providing sensitivity above 1050 Å. The overall spectral coverage of the instrument ranges thus from 905 to 1187 Å, and allows detection of the full Lyman line series with the exception of Lyα. Moreover, each channel uses two detector segments A and B. This results in eight spectral segments which are then co-added in the reduction process to obtain the final spectra (see e.g., Barstow et al. 2003). The observations are summarized in Table 2, which provides information on the number of exposures as well as on the total integration time. All spectra were taken using the 30"x 30" LWRS aperture, which provides a resolution of $\sim$ 20,000. The spectra were obtained either using the timetag (TTAG) or histogram (HIST) mode depending on the brightness of the object. In the present study, four program stars were observed using the HIST mode, while the remaining six were obtained using the TTAG mode. The data are then reduced using the most recent CALFUSE pipeline version available. The spectra were binned over 0.1 Å, as was done by Barstow et al. (2001), to augment the signal-to-noise ratio without loss of spectral definition. Moreover, some

FUSE spectra show strong emission lines due to the Earth's geocorona. These generally occur in the line cores and are ignored. Another artifact that must be dealt with is the absorption of interstellar H I. This may engender an artificial deepening of the line cores. It is possible for these effects to cancel each other, however, it is more appropriate to remove these regions from the data (Barstow et al. 2001). The spectra are shown in Figure 3.2 and appear in the same order as Figure 1. For two objects, PG 1710+490 and PG 1716+426, the data between 1120 Å and 1160 Å were problematic and were not considered in the reduction process. The omission of this spectral region does not affect our analysis as we can still detect the full Lyman series from Lyβ onwards. The ultraviolet spectra also feature numerous narrow lines of heavy elements, the influence of which will need to be considered. Overall, the shape of the absorption features is much rounder and broader for stars with $T_{\rm eff} < 30,000$ K, while the hotter stars have features that are sharper and narrower.

3.4 Model Calculations

The optical spectra of our sample objects show no strong features besides transitions of H I, He I, and He II. Accordingly, we calculated a grid of pure hydrogen models, as well as a grid of mixed helium and hydrogen models using an average helium abundance of log(He/H) $= -2.5$. This value corresponds to the mean helium abundance found in the literature. We use this second grid to verify the impact of a small helium abundance on the determination of our atmospheric parameters. The Napiwotzki (1997) analysis shows that the divergences between hydrogen and mixed compositions decrease as one goes from LTE to NLTE and as one goes to lower effective temperatures. Since we use NLTE models and restrict ourselves to relatively low temperatures, we do not expect large differences between our two grids of models in the results presented in § 5. Line blanketed LTE and NLTE models were calculated using version 200 of TLUSTY (Hubeny 1988), under the assumption of a plane parallel geometry and of hydrostatic and radiative equilibrium. The corresponding synthetic spectra were calculated with version 48 of SYNSPEC (Hubeny & Lanz 1995) and the Stark broadening tables of Lemke (1997) were used. We emphasize that no blanketing due to heavy elements is included in our initial model grids. The importance of this omission will be discussed in the following section.

Our model grids extend over the following range of parameters in each case: $T_{\rm eff} = 20,000$ K to 60,000 K spaced by 2000 K, $\log g = 5.0$ to 6.0 spaced by 0.25 dex. The calculations used 300 depth points for the pure H and 100 depth points for the mixed H-He models. All optical synthetic spectra were convolved with a Gaussian of full width at half maximum of 6 Å, while non-convolved spectra were used for the Lyman line analysis.

3.5 NLTE vs LTE and the Importance of Line Blanketing from Heavy Elements

Napiwotzki (1997) reports that for model atmosphere calculations of sdB stars, one must consider two important factors: NLTE effects and line blanketing from heavy elements. Past studies of the atmospheric properties of subdwarf B stars have frequently employed LTE models, but the results of Napiwotzki (1997) suggest an increase in NLTE effects for objects with $T_{\rm eff} > 30,000$ K. To verify the impact of NLTE effects, we used our pure hydrogen NLTE grid to derive the corrections in the values of $T_{\rm eff}$ and log g that need to be applied to the results of LTE analyses. These correction vectors are shown in Figure 3.3. For temperatures above 30,000 K, differences can be as large as 20,000 K and 0.5 dex, in the sense that the LTE generally underestimates these parameters.

Another important consideration is that of line blanketing (see e.g., Lanz et al. 1997; Brown et al. 1996). Findings report that simple mixed hydrogen/helium model calculations tend to overestimate effective temperatures, since line blanketing increases the opacity in the atmosphere and results in the cooling of the stellar surface and heating of the deeper layers through backwarming. Hence, neglecting the opacity of heavy elements such as iron, leads to NLTE models predicting too large a continuum flux, particularly in the FUV region, since it is there that most features from heavy elements are visible (Lanz & Hubeny 2003). Unfortunately, the heavy element abundances observed in sdB stars vary from object to object and do not necessarily follow solar or scaled solar abundance patterns. Thus, at this stage, we opted to include blanketing of hydrogen and helium, and heavy elements were not considered in our initial investigation.

3.6 Fits to the Balmer Lines

To determine the atmospheric parameters, $T_{\rm eff}$ and $\log g$, of our sample stars, we used the Balmer line fitting technique. The procedure can be summarized as follows: the observed and theoretical Balmer line profiles (Hβ-H9) are normalized to a linear continuum set to unity. The observations are then compared to synthetic spectra generated from model atmospheres. A chi-squared minimization technique is then applied until a best fit is achieved between the calculated model and the observations (see Holberg et al. 1985; Bergeron et al. 1992). We first proceeded using the pure hydrogen model grid, and obtained satisfactory fits. These are shown in Figure 3.4. The fits are presented in order of increasing temperature from left to right. We see that the line profiles are well reproduced. Furthermore, the values of $T_{\rm eff}$ and $\log g$ we determine are consistent with those found in the literature. We present, in Table 3, the derived effective temperatures, surface gravities, distances (in parsec), as well as abundances of helium and some heavier elements found in the literature. The distances were derived using the relation

$$f_\nu = 4\pi \frac{R^2}{D^2} H_\nu \,, \tag{3.1}$$

with a fixed mass $M = 0.55\ M_\odot$ for all of our objects. Reddening was not included in the calculation of the distances, as its influence is negligible in the visible domain. On the other hand, it becomes important in the FUV region, and these effects will be discussed in section 6.1.

3.6.1 The Impact of the Helium Abundance

As previously mentioned, we computed a mixed helium and hydrogen NLTE grid with $\log({\rm He/H}) = -2.5$ and refit all our optical spectra with that grid. The derived atmospheric parameters were quite similar to those obtained with the pure hydrogen grid and, in addition, the He I line profiles were well reproduced at the abundance chosen. The values of $T_{\rm eff}$ and $\log g$ obtained with the mixed grid are contrasted to the earlier values in Table 4. The values obtained with the mixed grid are generally hotter than their counterparts, except for HD 4539

and Ton S−227, and differ from them by 250 K at most. As for the gravities, they are generally larger for the fits with mixed models, by up to 0.013 dex. This reinforces the Napiwotzki (1997) claim that, if one uses NLTE models, the influence of helium is not dramatic. In what follows, we adopted the parameters obtained with the pure hydrogen grid.

3.7 The Lyman Lines

Although the analysis of the Lyman lines is patterned on work carried out on DA white dwarfs, there are substantial differences to be reckoned with: while DA white dwarfs show few lines in the FUSE spectral region, the ultraviolet spectra of subdwarf B stars are contaminated by hundreds of transitions from heavy elements (see, e.g, Ohl et al. 2000). These lines contribute to the overall blocking effect and must be considered when trying to fit the continuum, a crucial step in the fitting procedure. The problem could be alleviated were one to use synthetic spectra that include the line blanketing of heavy elements, but this task is complicated since the abundance patterns of heavy elements in sdB stars are inhomogeneous, and are still being documented (Fontaine et al. 2005). We show in Figure 3.5 the results of this experiment for two typical objects in our sample. Firstly, we note that the continuum is placed by taking an average of the "noise", that is in reality the numerous lines of heavy elements. Moreover, elements such as iron contribute to the overall line blocking effect and depress the flux in the FUV region (Brown et al. 1996). Thus, one cannot accurately determine the level of the continuum, and consequently the derived parameters tend to be inconsistent with the optical values.

Faced with this situation, we adopted a different approach in which we look for consistency between the optical parameters and the fluxes observed in the FUSE range. To do this, we use the $T_{\rm eff}$ and $\log g$ derived from the optical spectra to interpolate the synthetic spectra in the FUSE range. These spectra are normalized through the observed Strömgren y magnitude. The Strömgren y index is used to calculate the observed flux at 5458.7 Å with the following relation

$$f_\lambda = 3.61 \times 10^{-9} \times 10^{-0.4y} \tag{3.2}$$

It is then possible to obtain a value for the solid angle and normalize the emergent flux of our model spectrum. The results of this procedure are shown in Figures 3.6 and 3.7 for our nine sample objects. They appear in order of increasing temperature from bottom up.

Overall, the match between the synthetic spectra and the ultraviolet continuum and Lyman lines goes from quite satisfactory to poor. Because there are several reasons we can identify for this spread, we discuss in greater detail, in the following sections, our initial findings, as well as certain avenues that do help provide an improved consistency between the predicted spectra and the observations. Incidently, as we will see, our results may provide a way to place the continuum level in abundance analyses of sdB stars — a point of some interest in current studies.

3.7.1 A First Look at the Results

Upon first inspection, the agreement for the lower temperature objects appears quite good when some allowance is made for line blocking from heavy elements which is left out from our model grid. For the two coolest objects in Figure 3.6, HD 4539 and PG 1716+426, both at $T_{\rm eff} < 27,000$ K, there is a good match between the predicted synthetic spectra and the FUSE data: the Lyman lines are well fit while the continuum level is consistent with the predicted flux, in the sense that the observed departures appear reasonable given the expected effect of line blocking from heavy elements. As we describe in detail below, the continuum level can be affected by interstellar extinction and it behooves us to look at its importance for each individual object. Upon examination of the reddening maps of Burstein & Heiles (1982) we find that there is a maximum extinction of $E(B-V) = 0.22$ on the line of sight to HD 4539. However, HD 4539 is so bright that it is a fairly nearby object ($d = 215$ pc), and the true extinction is likely to be much less than that value. In the case of PG 1716+426, the extinction maps show very little extinction on its line of sight, although it lies at a much greater distance of 1.1 kpc.

For the intermediate temperature stars in our sample, at $T_{\rm eff} < 31,000$ K, the differences between the predicted and observed fluxes appear too important to be explained simply by the lack of line bocking from heavy elements in our synthetic spectra. This is the case, for

example, for PHL 457, and we suspect that this discrepancy is associated with the omission of reddening in our initial fits. We discuss the reddening correction and our improved results in the following section. We find that reddening appears to be an important factor for four of our programme stars: PHL 457, PG 1743+477, PG 1710+490, and PG 0823+466.

The hottest stars in our sample, such as Ton S−227, present what appears to be a different problem. More specifically, the predicted Lyman lines appear too wide, particularly from Lyγ onwards, while the flux in the interline region appears too low. This discrepancy between the synthetic spectrum calculated with the optical parameters and the observed ultraviolet spectrum is present for all objects with $T_{\rm eff} > 31,000$ K (namely PG 1032+406, Ton 13, and Ton S-227) and appears more difficult to explain. Moreover, the observed effect appears to worsen as the temperature increases. The poorly reproduced Lyman lines lead one to believe that the surface gravity determined in the optical might be too high, an admittedly worrisome result for asteroseismological studies of sdB stars, while the low level of the predicted continuum is difficult to account for given the expected presence of some line blocking. We explore plausible sources for this disagreement and present them in the following subsections.

3.7.2 Interstellar Extinction and the Intermediate Temperature Objects

For the high galactic latitude objects in our sample, the y magnitude used to normalize our energy distribution is not likely to be affected significantly by interstellar extinction. The situation is different in the far ultraviolet, however, and the effect of small values of $E(B-V)$ on the energy distribution of hot subdwarfs and even nearby white dwarfs is well documented (Heber 1986). We suspect that interstellar extinction might be a factor in the marginal agreement obtained in our intermediate temperature stars, and we explore this possibility here by applying the Seaton (1979) reddening curve to our synthetic spectra calculated at the atmospheric parameters derived in the optical.

For PHL 457, Heber (1986) gives a limit on the color excess of $E(B-V) < 0.05$. Our tests, shown in Figure 3.8, show that a smaller value of $E(B-V) = 0.02$ is sufficient to bring the far-ultraviolet spectrum in much better agreement with the FUSE data than was previously possible. For PG 1743+477, Moehler et al. (1990) determine a color excess $E(B-V) = 0.03$

on the basis of a comparison of the observed colors with those predicted on the basis of the values of $T_{\rm eff}$ and $\log g$ determined for that star. When that correction is applied to our synthetic far-ultraviolet spectra, the agreement with the observed data is greatly improved (Fig. 3.8). The profiles are more accurately reproduced, particularly the wing regions and the continuum, despite some line blocking, is also in satisfactory agreement. For PG 1710+490, the maps of Burstein & Heiles (1982) yield a maximum value of 0.02, a value consistent with those derived in the literature for this object. Here again, a much more consistent adjustment is possible with a small value of the color excess. The last problematic object in our list is PG 0823+466. Since this object did not have a published $E(B-V)$ value, we first estimated it using the same procedure as Moehler et al. (1990), that is, using $BVRI$ photometry we compare the observed colors to models for the derived parameters. Thus the colors of a model of 30,000 K and log g 5.75 are deemed comparable to the 30,602 K and 5.675 derived for PG 0823+466 and we obtain $(B-V) = -0.25$ while the observed $(B-V) = -0.18$ (Kilkenny et al. 1988), resulting in an approximate color excess $E(B-V) = 0.07$ for this object located at 1.1 kpc. The maximum extinction listed by Burstein & Heiles (1982) for these coordinates is a consistent value of $E(B-V) = 0.096$. This correction improves the result considerably, even though the final match is not as satisfactory as in the previous objects.

Finally, we also looked at how reddening affects the hotter objects in our sample. On the one hand, values found in the literature suggest very little reddening for these objects while, on the other, reddening of the synthetic spectra goes in the opposite direction to that required, since the predicted continuum level is already too low. Other phenomena must play an important role. The explanation of the hotter objects must thus lie elsewhere.

3.7.3 The Hot Objects

The problem encountered for objects with $T_{\rm eff} > 31,000$ K is similar to that reported by Brown et al. (1996). Namely, the predicted Lyman lines are too strong when compared to the observed profiles, while the predicted continuum flux is too low. This systematic discrepancy implies that either the surface gravity value determined from the optical observations is too large or, alternatively, that the effective temperature is too low. A similar effect was found by

Barstow et al. (2003) for DA white dwarfs. These suspicions are confirmed by the experiment shown in Figure 3.9 for Ton S−227. There, we show the match obtained by adopting the optical effective temperature while adopting a lower surface gravity than obtained in the optical. The bottom part of the figure shows the inverse experiment, namely adopting the optical surface gravity while adopting a higher effective temperature than obtained in the optical. The required changes are of the order of -1 dex in $\log g$ or, alternatively, 3500 K in effective temperature. In either case, the match with the observed data is improved. However, this does not explain why the usually reliable optical determinations of atmospheric parameters should be that far off the mark for the stars above 31,000 K.

Since the importance of line blanketing from heavy elements has been made evident in various papers, such as Napiwotzki (1997) and Lanz et al. (1997), it was imperative that we explore these effects for our objects. As a preliminary test, we were kindly provided with pure hydrogen and solar abundance model atmospheres calculated by N. Behara using the model atmosphere code STERNE (Jeffery & Heber 1992). We used these models along with SYNSPEC to generate synthetic spectra with $T_{\rm eff} = 34,000$ K and $\log g = 6.0$, typical of those appropriate for Ton S-227. We then used our Balmer fitting procedure and our own grid of model synthetic spectra to determine effective temperatures and surface gravities. These results are shown in Figure 3.10, where we fit both the pure hydrogen and the solar abundance spectra as if they were observed spectra. We find in both cases parameters close to their nominal values: the pure hydrogen fit tests the consistency between Behara's atmospheric structure and our own TLUSTY structure for a pure hydrogen composition ($\Delta T_{\rm eff} = 49$ K, $\Delta \log g = 0.05$ dex), while the solar abundance fit ($\Delta T_{\rm eff} = -1030$ K, $\Delta \log g = 0.19$ dex) confirms that the securing of atmospheric parameters through traditional Balmer line fits provides robust results, nearly independent of the photospheric abundance of heavy elements.

The following step was to examine the synthetic spectra in the far-ultraviolet region. In Figure 3.11, we superpose a synthetic spectrum with $T_{\rm eff} = 34,000$ K and $\log g = 6.0$ computed with the TLUSTY (dashed line) stratification onto the one computed with the STERNE stratification (solid line) for both abundances. The top panel shows the pure hydrogen results: the consistency observed earlier between the TLUSTY and STERNE stratifications for the

same pure hydrogen composition also extends to the far ultraviolet. However, the situation is clearly different for the solar abundance spectrum (bottom panel): the Lyman lines in the solar abundance model are narrower, and the continuum flux level is higher than in the pure hydrogen model. This is similar to the the effect observed in our matches to Ton S−227 and its siblings, a result which suggests that the source of the poor matches in PG 1052+406, Ton 13, and Ton S−227 is related to the line blanketing (as opposed to simple line blocking) associated with the heavy elements.

Our conclusions, at this stage, must remain qualitative since we are currently unable to explore these blanketing effects with large grids of models. The next steps will obviously include the exploration of compositions scaled with respect to the solar one, and even of variations in individual abundances (for example, for individual iron-peak elements) with respect to the average scaled value. Ultimately, when these diverse grids become available, we believe we will be in a position to actually fit — as opposed to match — the far ultraviolet spectrum. Indeed, because the line blanketed models include both the blocking and the backwarming effects expected from numerous lines of heavy elements, only then will the original idea of fitting the ultraviolet continuum with the traditional chi-squared minimization technique become a reality.

3.8 Conclusions

The comparison of derived parameters from optical and far-ultraviolet spectra can provide a useful consistency check for the analysis of sdB stars. However, in the present study, we show that several factors render this task difficult to accomplish at this time. Namely, poorly known abundances and the relative difficulty to compute model atmospheres with the full blanketing of heavy elements are key issues that must be resolved. We have thus developed a different approach in which we derive atmospheric parameters ($T_{\rm eff}$ and $\log g$) using the standard Balmer line fitting procedure and use these values, along with Strömgren y magnitude, to predict synthetic spectra in the ultraviolet.

We initially find good agreement for low temperature objects ($T_{\rm eff} < 27,000$ K), while intermediate temperature stars ($27,000$ K $< T_{\rm eff} < 31,000$ K) and high temperature stars

($T_{\rm eff} > 31,000$ K) show obvious discrepancies. We find that in the case of four of our programme stars, PHL 457, PG 1743+477, PG 1710+490, and PG 0823+466, the inclusion of small amounts of interstellar reddening results in a significant improvement in the match. As for the hotter objects in our sample, we explore the influence of line blanketing from heavy elements for a restricted number of model atmosphere models ($T_{\rm eff} = 34,000$ K and $\log g = 6.0$ dex) in both spectral regions. We find that firstly, pure hydrogen, NLTE model atmospheres do indeed provide reliable temperature and gravity estimates for optical observations, while the lack of heavy elements in our model calculations could be an important source of error in the match to the far-ultraviolet region. Initial findings show that a solar abundance model at our nominal $T_{\rm eff}$ and $\log g$ values results in narrower lines and a higher flux level. This suggests strongly that the poor matches obtained for our hotter objects could be due to the lack of line blanketing by heavy elements in our models.

We thank the director and staff of the Steward Observatory for the use of their facilities. We also thank N. Behara for the use of her models and P. Chayer for useful discussions pertaining to this project. This work was supported in part by the NSERC Canada and by the Fund FQRNT (Québec).

TABLEAU 3.1 – Sample Objects

Name	Other Names	y-mag	References
HD 4539	PG 0044+097	10.31	(1)
PG 1716+426		13.97	(2)
PHL 457	GD 1110	12.95	(3)
PG 1743+477		13.79	(2)
PG 1710+490		12.90	(2)
PG 0823+466		14.53	(2)
PG 1032+406		11.52	(2)
Ton 13	PG 0919+273	12.77	(2)
Ton S−227	PHL 1126, GD 1319	11.76	(1)

References. – (1) Bergeron et al. (1984); (2) Wesemael et al. (1992); (3) Kilkenny et al. (1977)

TABLEAU 3.2 – FUSE Data

Name	Program ID	Date	Number of Exposures	Total Exposure Time (sec)	Aperture	Mode
HD 4539	B0540201000	2001-07-17	1	59	LWRS	HIST
PG 1716+426	B0541301000	2002-09-09	5	6074	LWRS	TTAG
PHL 457	E1221201000	2004-07-15	9	10143	LWRS	TTAG
PG 1743+477	Z9043401000	2002-07-16	2	6686	LWRS	TTAG
PG 1710+490	B0541101000	2002-09-09	2	4630	LWRS	TTAG
PG 0823+466	Z9041001000	2004-03-19	7	6720	LWRS	TTAG
PG 1032+406	B0540501000	2001-05-01	9	3948	LWRS	HIST
Ton 13	P2050201000	2001-05-02	23	9870	LWRS	HIST
Ton S−227	B0540601000	2001-08-07	12	6518	LWRS	HIST

TABLEAU 3.3 – Derived Parameters

Name	$T_{\rm eff}$ (K)	$\log g$	Dist (pc)	log(He/H)	C	N	Si	Fe
HD 4539	24,089	5.211	215.5	−2.27	−3.9	−4.0	−5.2	−4.8
PG 1716+426	26,919	5.335	1110.0	−3.01	**	**	**	**
PHL 457	27,246	5.364	680.5	−2.49	**	**	**	**
PG 1743+477	27,676	5.518	851.1	−2.16	**	**	**	**
PG 1710+490	29,864	5.652	524.5	−2.43	−4.8	−4.0	−4.8	−4.3
PG 0823+466	30,602	5.675	1110.0	−2.70	**	**	**	**
PG 1032+406	31,012	5.802	243.1	−2.30	−5.3	−4.6	< -9.0	−5.8
Ton 13	32,158	5.801	448.0	−2.41	**	**	**	**
Ton S−227	34,437	5.947	253.5	−3.23	< -9.0	−4.6	< -9.0	−5.7

TABLEAU 3.4 – Hydrogen vs Helium

Name	$T_{\rm eff}$ (K)	$\log g$	$T_{\rm eff}$ (K)	$\log g$
HD 4539	24,089	5.211	23,962	5.198
PG 1716+426	26,919	5.335	27,077	5.339
PHL 457	27,246	5.364	27,394	5.364
PG 1743+477	27,676	5.518	27,765	5.505
PG 1710+490	29,864	5.652	30,108	5.654
PG 0823+466	30,602	5.675	30,841	5.682
PG 1032+406	31,012	5.802	31,198	5.805
Ton 13	32,158	5.801	32,283	5.804
Ton S−227	34,437	5.947	34,391	5.946

3.9 References

Barstow, M. B., Good, S. A., Burleigh, M. R., Hubeny, I., Holberg, J. B., & Levan, A. J. 2003, MNRAS, 334, 562

Barstow, M. B., Holberg, J. B., Hubeny, I., Good, S. A., Levan, A. J., & Meru, F. 2001, MNRAS, 328, 211

Bergeron, P., Fontaine, G., Lacombe, P., Wesemael, F., Crawford, D. L., & Jakobsen, A. M. 1984, AJ, 89, 374

Bergeron, P., Saffer, R. A., & Liebert, J. 1992, ApJ, 394, 228

Bergeron, P., Wesemael, F., Michaud, G., & Fontaine, G. 1988, ApJ, 332, 964

Brown, T. M., Ferguson, H. C., & Davidsen, A. F. 1996, ApJ, 472, 327

Burstein, D., & Heiles, C. 1982, AJ, 87, 1165

D'Cruz, N. L., Dorman, B., Rood, R. T., O'Connell, R. W. 1996, ApJ, 466, 359

Edelmann, H., Heber, U., Hagen, H.-J., Lemke, M., Dreizler, S., Napiwotzki, R., & Engels, D. 2003, A&A, 400, 939

Fontaine, G., & Chayer, P. 1997, in The Third Conference on Faint Blue Stars, ed. A. G. D. Philip, J. Liebert, & R. A. Saffer (Schnectady: Davis Press), p. 169

Fontaine, M., Chayer, P., Wesemael, F., Lamontagne, R., Blanchette, J.-P., & Fontaine, G. 2005, in Astrophysics in the Ultraviolet, ed. G. Sonneborn, H. W. Moos, & B.-G. Andersson, in press.

Good, S. A., Barstow, M. B., Holberg, J. B., Sing, D. K., Burleigh, M. R., & Dobbie, P. D. 2004, MNRAS, 355, 1031

Han, Z., Podsiadlowski, Ph., Maxted, P. F. L., Marsh, T. R. 2003, MNRAS, 341, 669

Han, Z., Podsiadlowski, Ph., Maxted, P. F. L., Marsh, T. R., Ivanova, N. 2002, MNRAS, 336, 449

Heber, U. 1986, A&A, 155, 33

Holberg, J. B., Wesemael, F., Wegner, G., & Bruhweiler, F. C. 1985, ApJ, 293, 294

Hubeny, I. 1988, Computer Physics Comm., 52, 103

Hubeny, I., & Lanz, T. 1995, ApJ, 439, 875

Iben, I. Jr., Tutukov, A. V. 1986, ApJ, 311, 735

Jeffery, C. S., & Heber, U. 1992, A&A, 260, 133

Kilkenny, D., Heber, U., & Drilling, J. S. 1988, South African Astron. Obs. Circ., 12, 1

Kilkenny, D., Hill, P. W., & Brown, A. 1977, MNRAS, 178, 123

Lanz, T., & Hubeny, I. 2003, ApJS, 146, 417

Lanz, T., Hubeny, I., & Heap, S. R. 1997, ApJ, 485, 843

Lemke, M. 1997, A&AS, 122, 285

Maxted, P. F. L., Heber, U., Marsh, T. R., North, R. C. 2001, MNRAS, 326, 1391

Michaud, G., Bergeron, P., Heber, U., & Wesemael, F. 1988, ApJ, 338, 417

Moehler, S., Heber, U., & de Boer, K. S. 1990, A&A, 239, 265

Moos, H. W. et al., 2000, ApJ, 538, L1

Napiwotzki, R. 1997, A&A, 322, 256

Ohl, R. G., Chayer, P.,& Moos, H. W. 2000, ApJ, 538, L95

Saffer, R. A., Bergeron, P., Koester, D., & Liebert, J. 1994, ApJ, 432, 351

Sahnow, D. J. et al., 2000, ApJ, 538, L7

Seaton, M. J. 1979, MNRAS, 187, 73P

Sweigart, A. V. 1997, ApJ, 474, L23

Unglaub, K., & Bues, I. 2001, A&A, 374, 570

Vennes, S., Chayer, P., Dupuis, J, & Lanz, T. 2005, in ASP Conf. Ser., 14th European Workshop on White Dwarfs, ed. D. Koester & S. Moehler (San Francisco: ASP), 185

Wesemael, F., Allard, F., Lamontagne, R., Fontaine, G., and Bergeron, P. 1997, in Proc. of The Third Conference on Faint Blue Stars, eds. A. G. D. Philip, J. Liebert, & R. A. Saffer (Schenectady: L. Davis Press), p. 433

Wesemael, F., Fontaine, G., Bergeron, P., Lamontagne, R., & Green, R. F. 1992, AJ, 104, 203

3.10 Figures

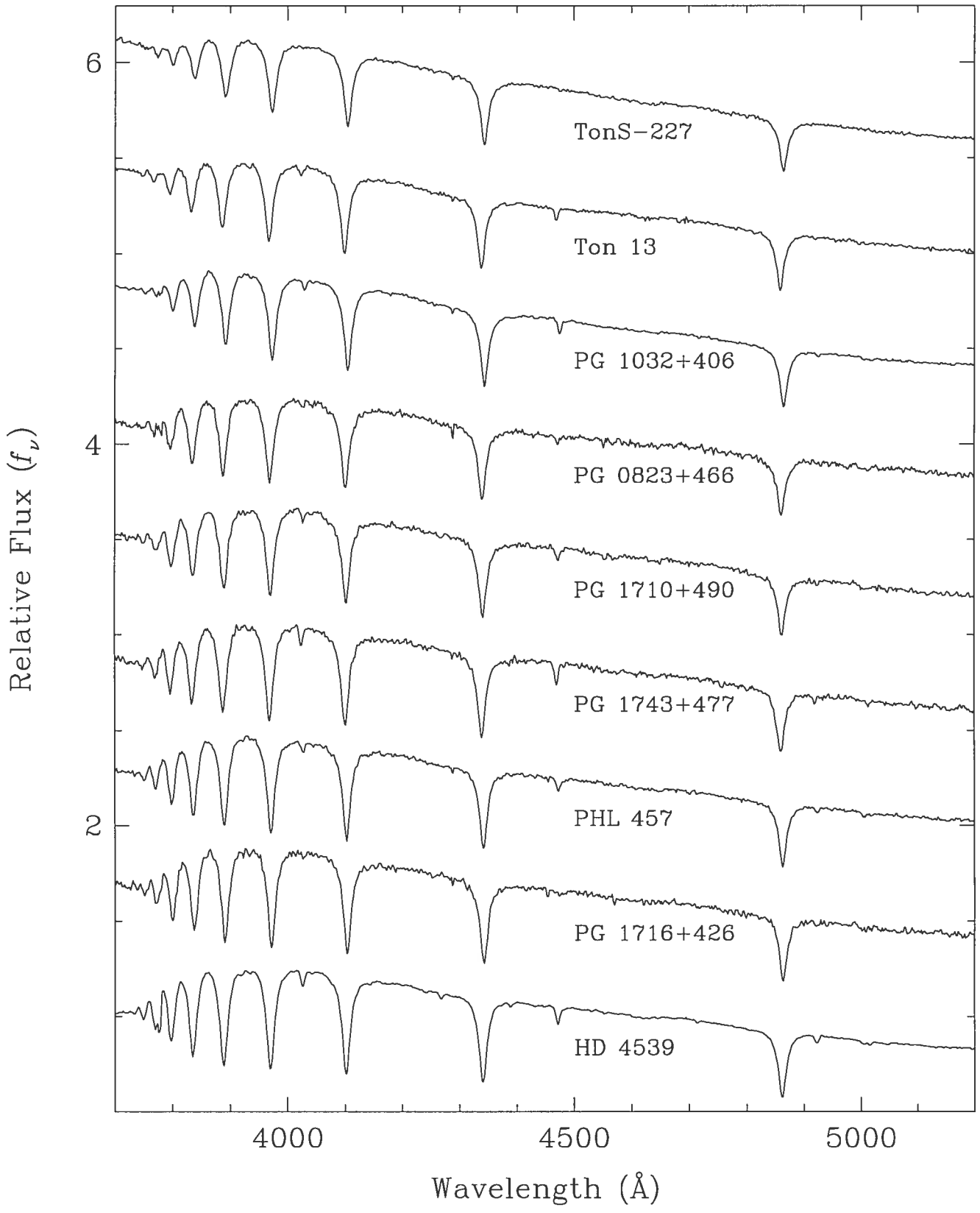

FIGURE 3.1 – Optical spectra of our sample objects. They appear in order of decreasing temperature from top to bottom and have been flux-calibrated, normalized to unity at 4600 Å and offset from each other by a factor of 0.60 for clarity.

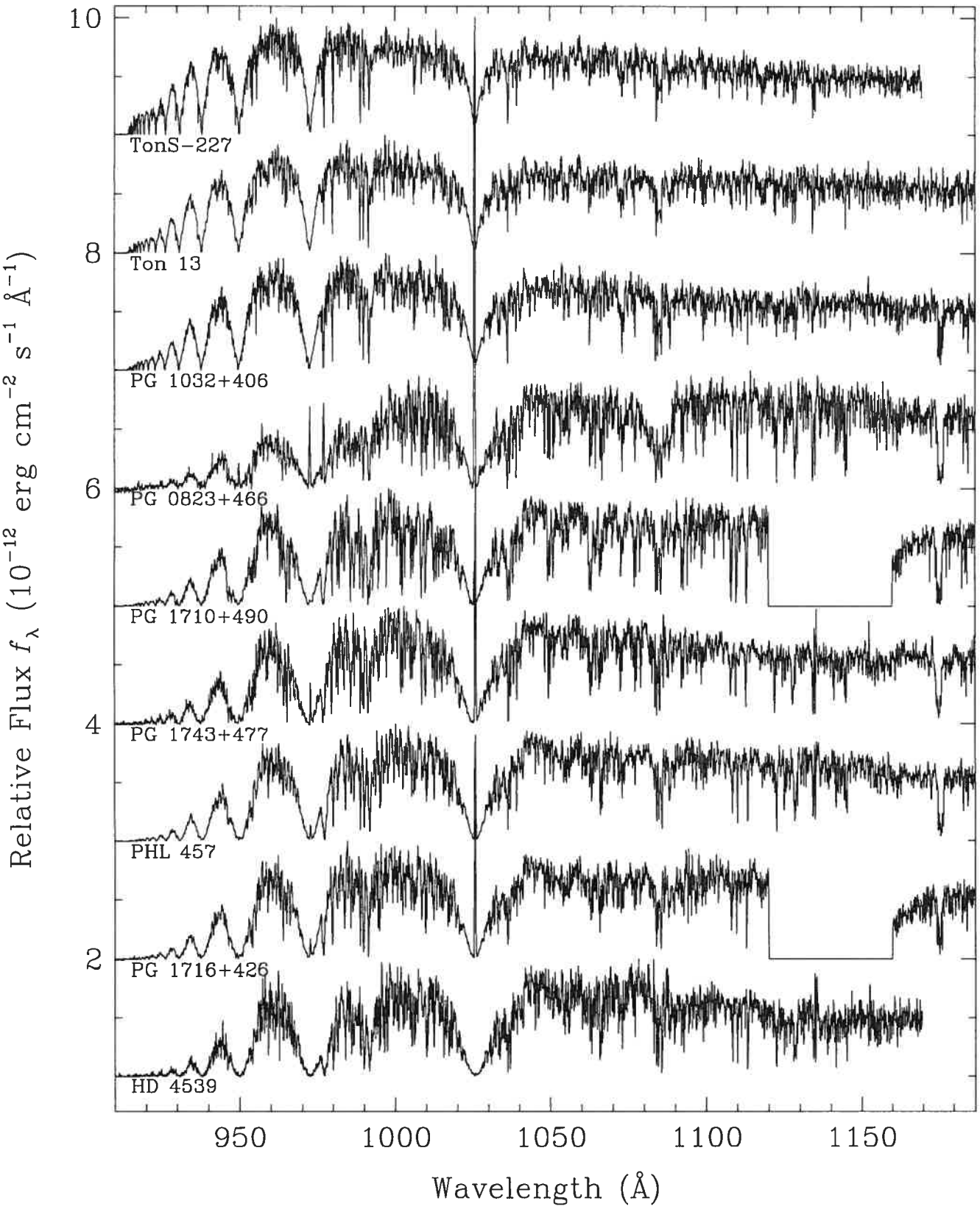

FIGURE 3.2 – *FUSE* spectra of our sample objects. They appear in order of decreasing temperature from top to bottom and have been reduced and calibrated using the CALFUSE pipeline. They are normalized to unity and offset from each other by a factor of 1.0 for clarity.

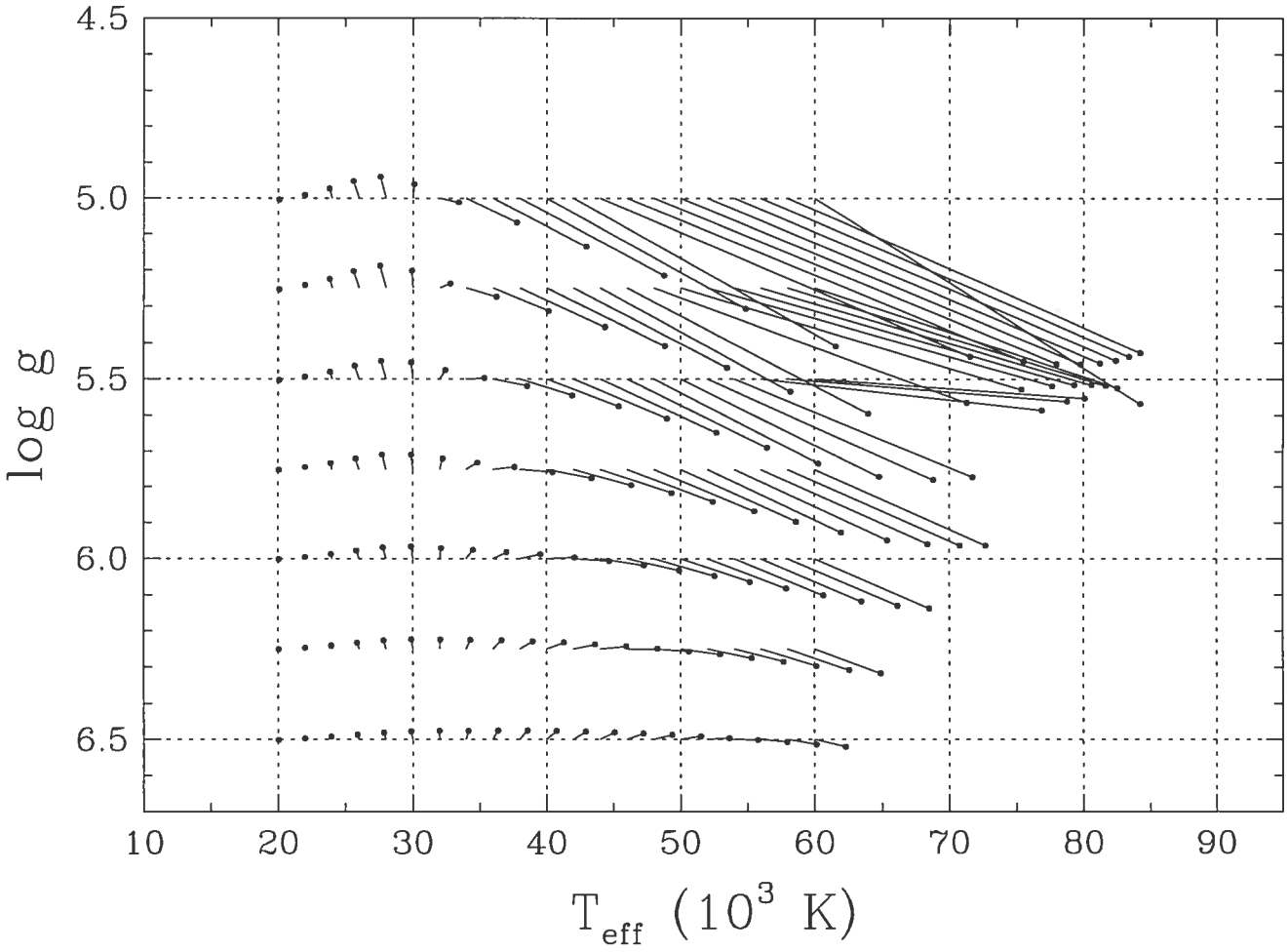

FIGURE 3.3 – Corrections that must be applied to LTE derived parameters to account for NLTE effects. Overall, LTE underestimates both $T_{\rm eff}$ and $\log g$.

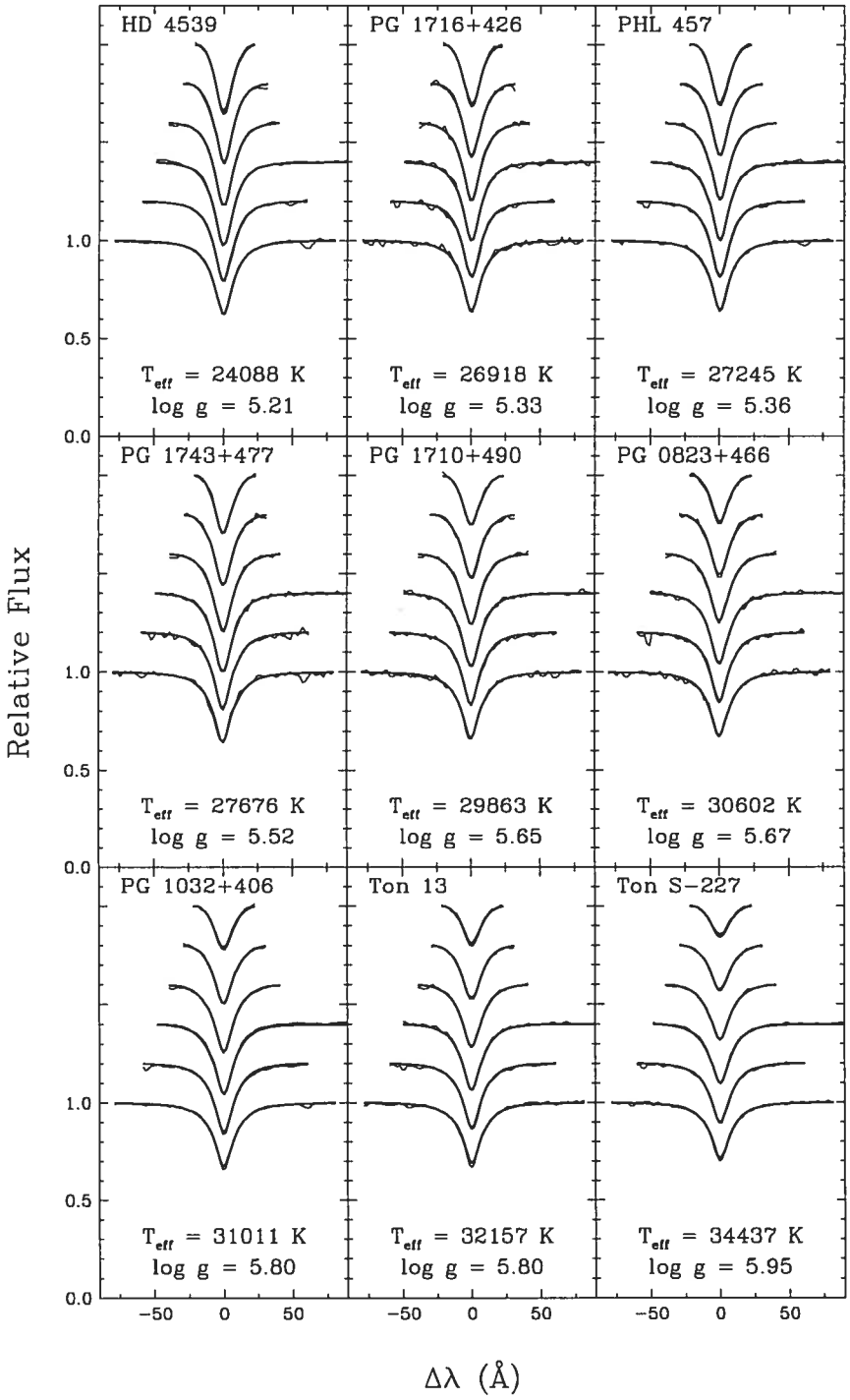

FIGURE 3.4 – Balmer line fits using our pure hydrogen NLTE model grid. The stars appear in increasing temperature from top left to bottom right and we show Hβ to H9. Overall, the line profiles are well reproduced.

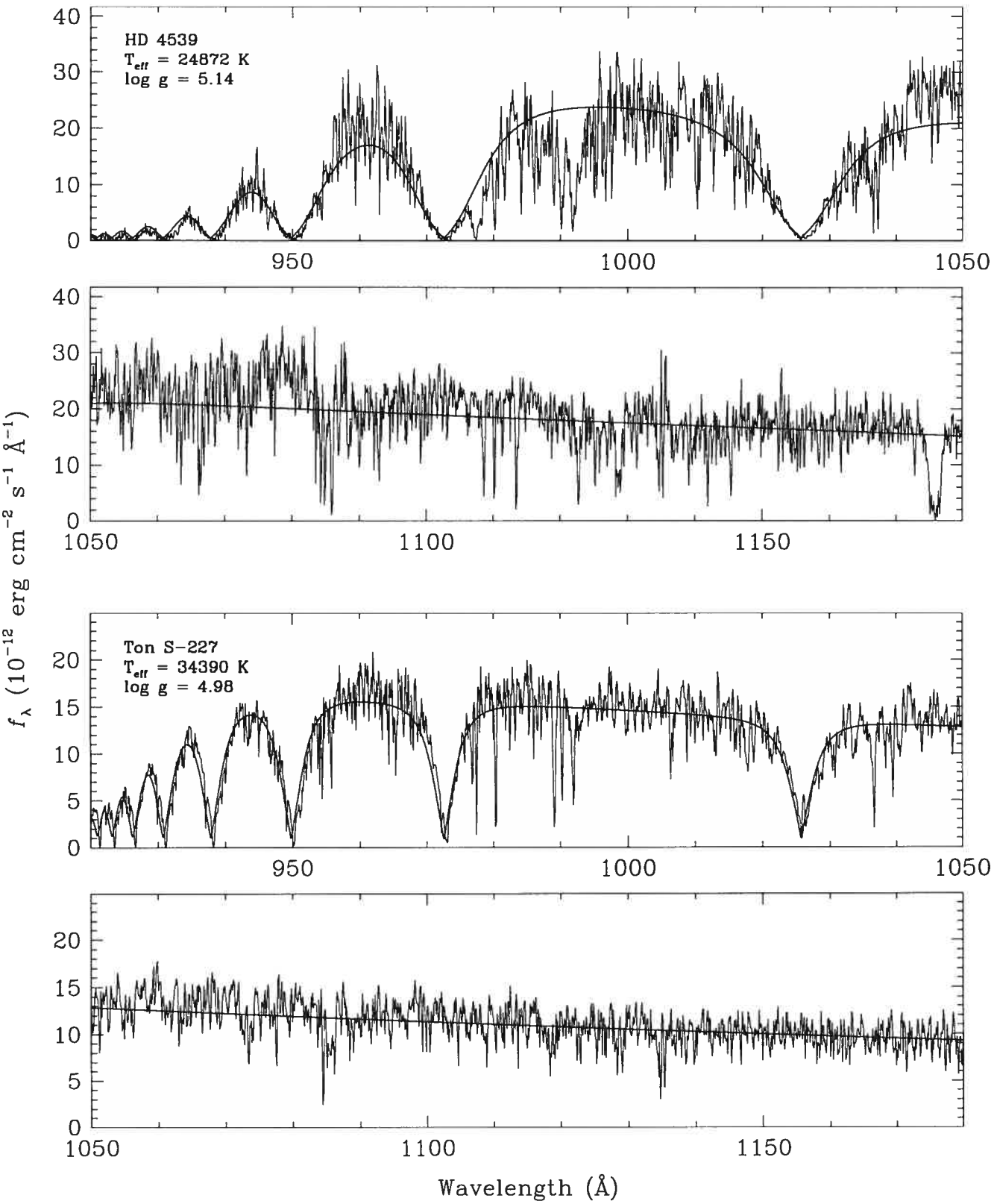

FIGURE 3.5 – First attempt at fitting Lyman lines using the same method as the Balmer lines. Here we use the NLTE pure H grid. We see that the placement of the continuum is taken through the average of the "noise"; however, this is not noise, but rather heavy element absorption features. Consequently the derived parameters are inconsistent with the optical values.

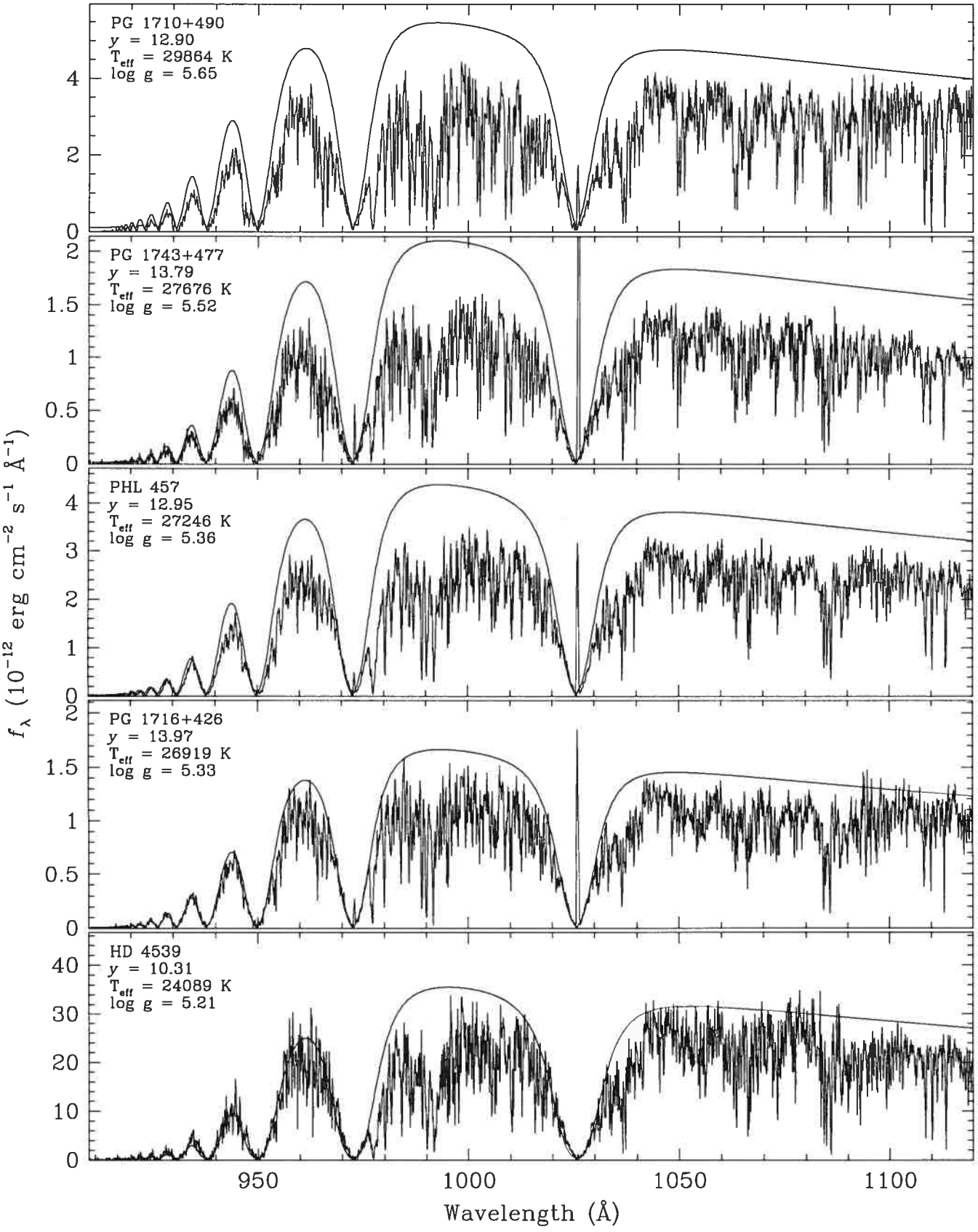

FIGURE 3.6 – Predicted ultraviolet spectra determined from Balmer line fits using our pure hydrogen NLTE model grid. We show our sample objects in order of increasing temperature from bottom up. We see that for cooler objects there is better agreement than for the hotter stars. Also, reddening has not been included in these initial predictions.

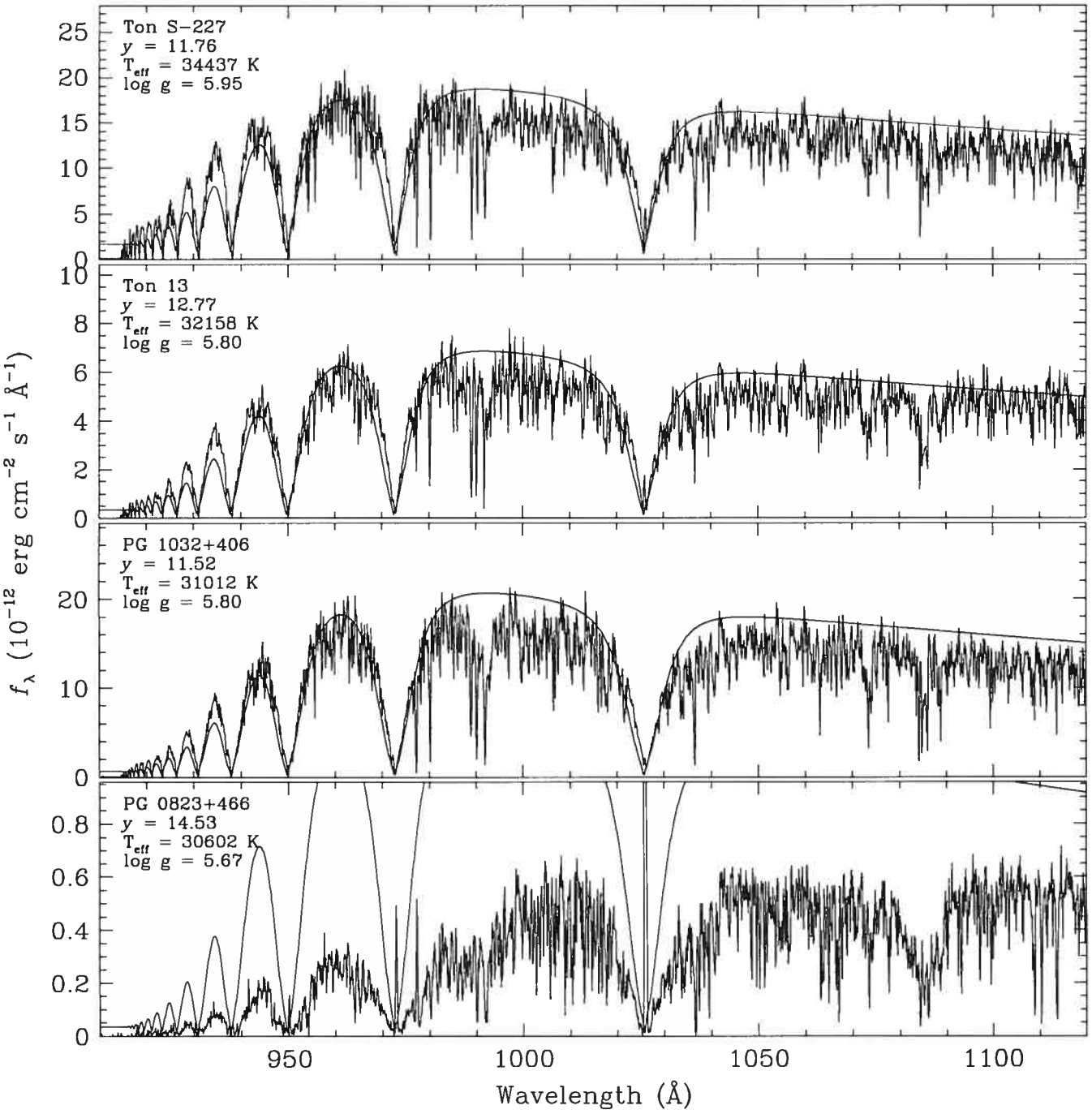

FIGURE 3.7 – Same as 3.6

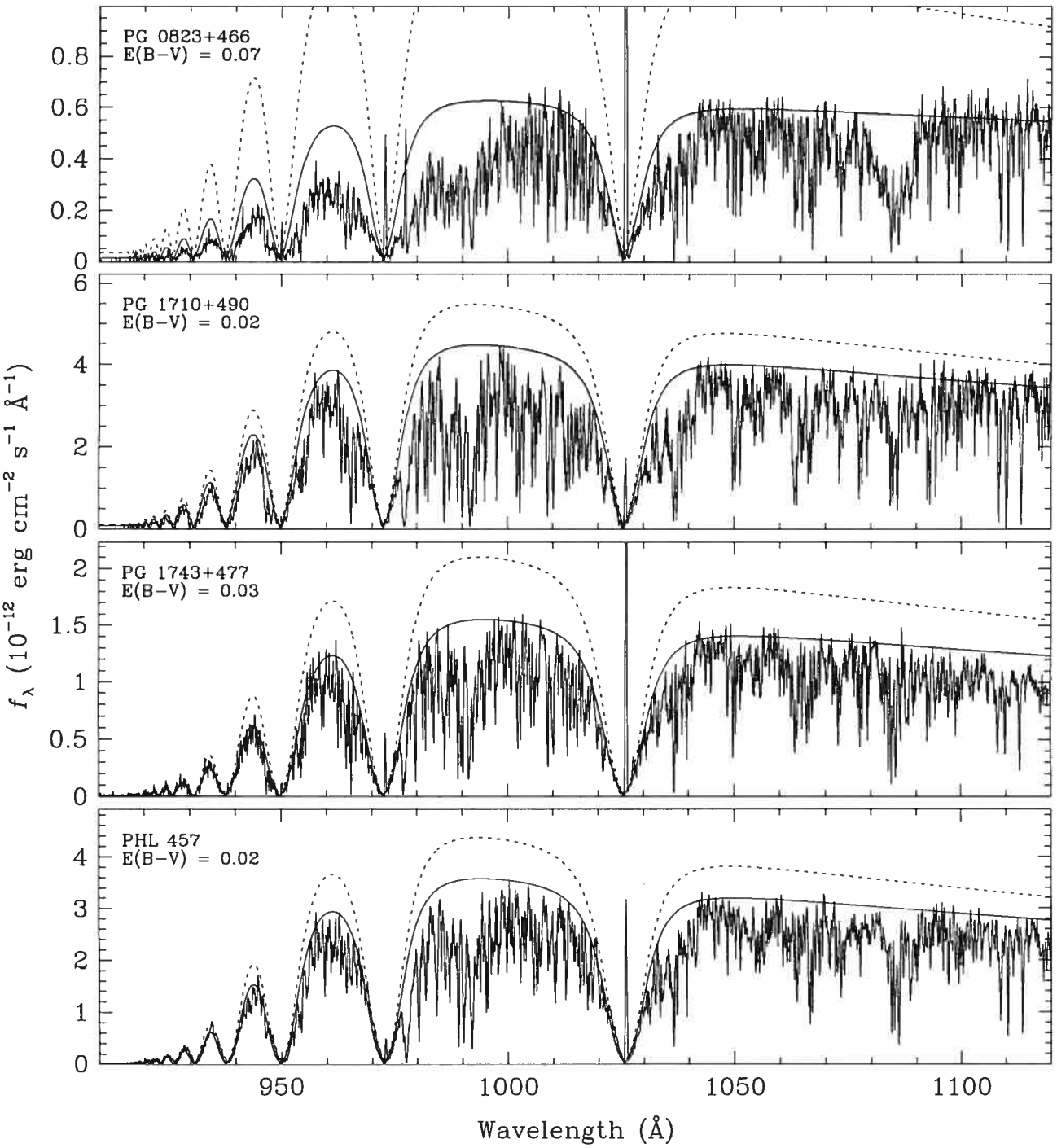

FIGURE 3.8 – Reddening corrections applied to four problematic sdBs. We see that including reddening can greatly improve the consistency of the predicted spectra with the *FUSE* observations. We have obtained values of $E(B-V)$ from the literature, and when these were not available, we estimated values using the reddening maps of Burstein & Heiles (1982) - see text. We see that even small amounts of extinction can have an important impact on the line profiles and continuum in the FUV region. The dashed line shows the original prediction, while the solid line applies the reddening correction of Seaton (1979). The $E(B-V)$ values are indicated in the top lefthand corner.

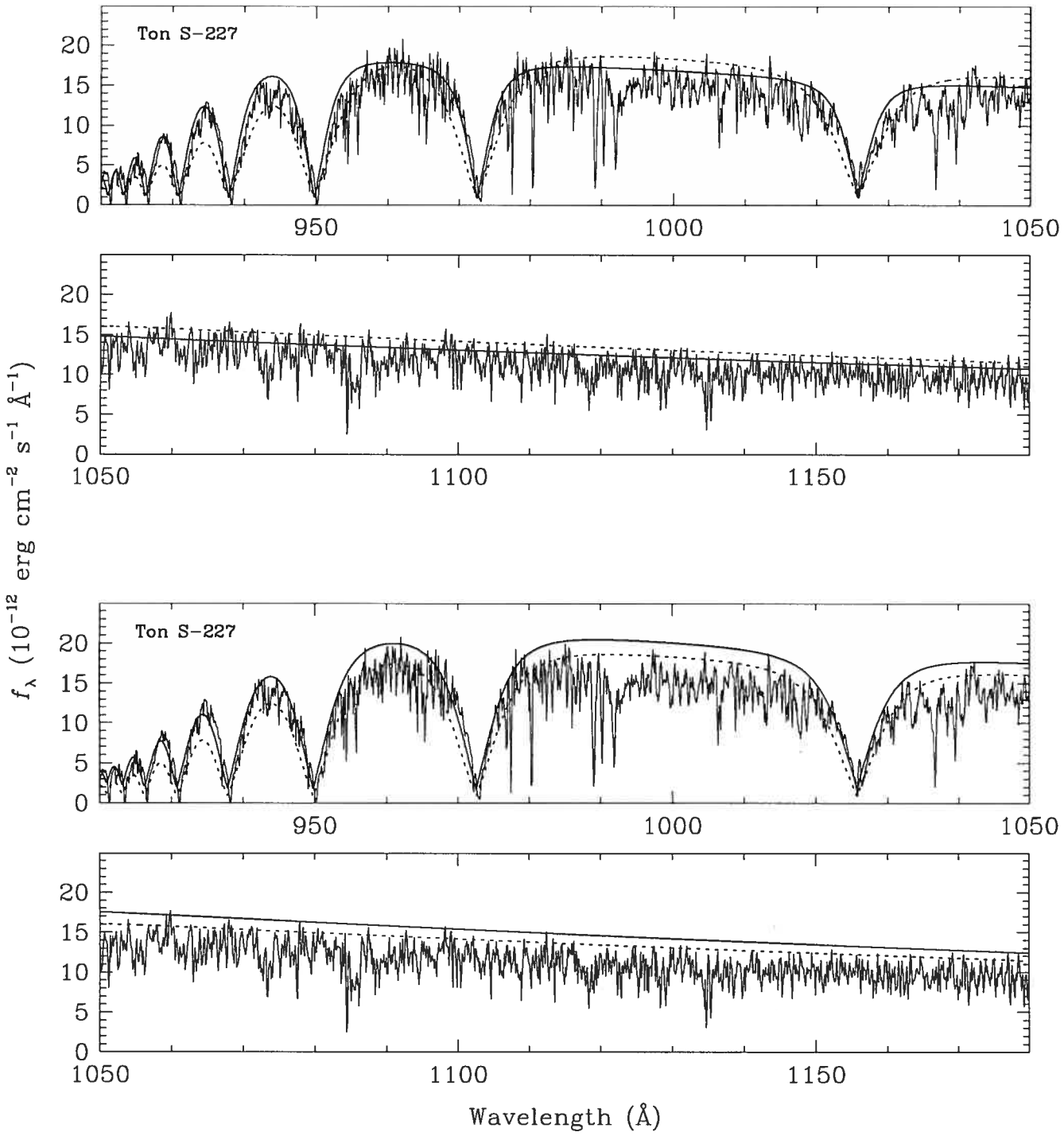

FIGURE 3.9 – Effects of varying $T_{\rm eff}$ and $\log g$ for Ton S−227. We show in the top panel the predicted spectra derived from the optical parameters $T_{\rm eff} = 34,437$ K and $\log g = 5.95$ (dashed line) versus a spectra for which we keep the effective temperature constant and vary the surface gravity until the model matches the observations. In this case $T_{\rm eff} = 34,437$ K and $\log g = 5.00$ (solid line). In the bottom panel we show the same experiment but keep the gravity constant and very the effective temperature. Hence, we show the original prediction with $T_{\rm eff} = 34,437$ K and $\log g = 5.95$ (dashed line) versus $T_{\rm eff} = 38,000$ K and $\log g = 5.95$ (solid line).

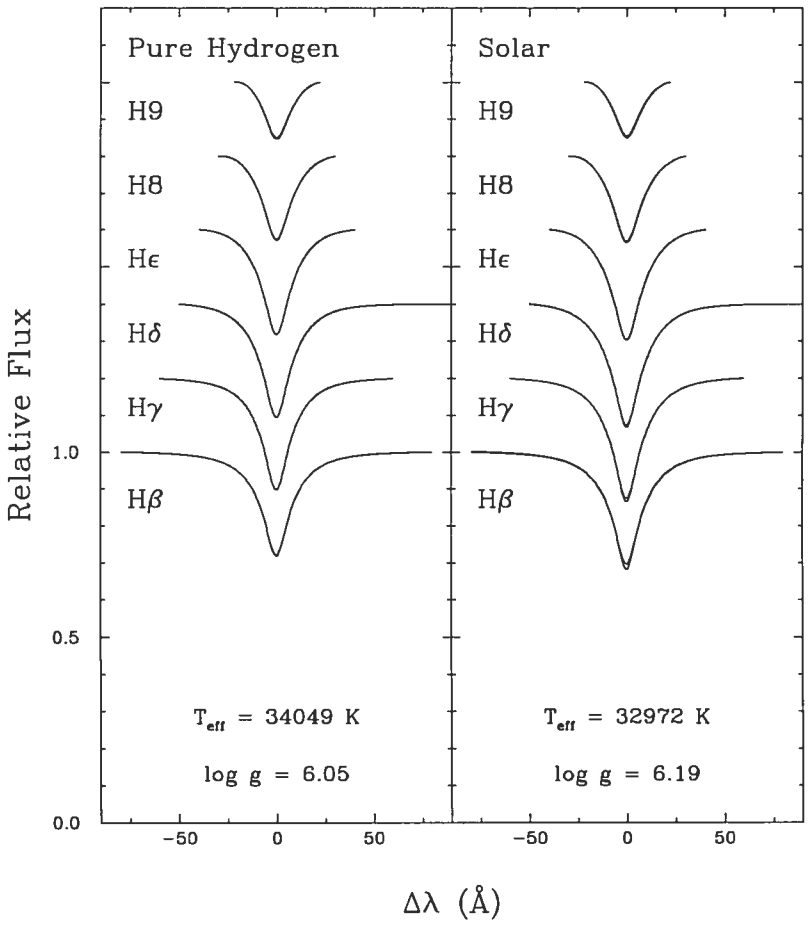

FIGURE 3.10 – Balmer line fit of STERNE synthetic spectra calculated for pure hydrogen (*left*) and solar abundance (*right*) and $T_{\rm eff} = 34,000$ K, $\log g = 6.0$. The spectra were convolved over 6 Å to be consistent with our optical observations.

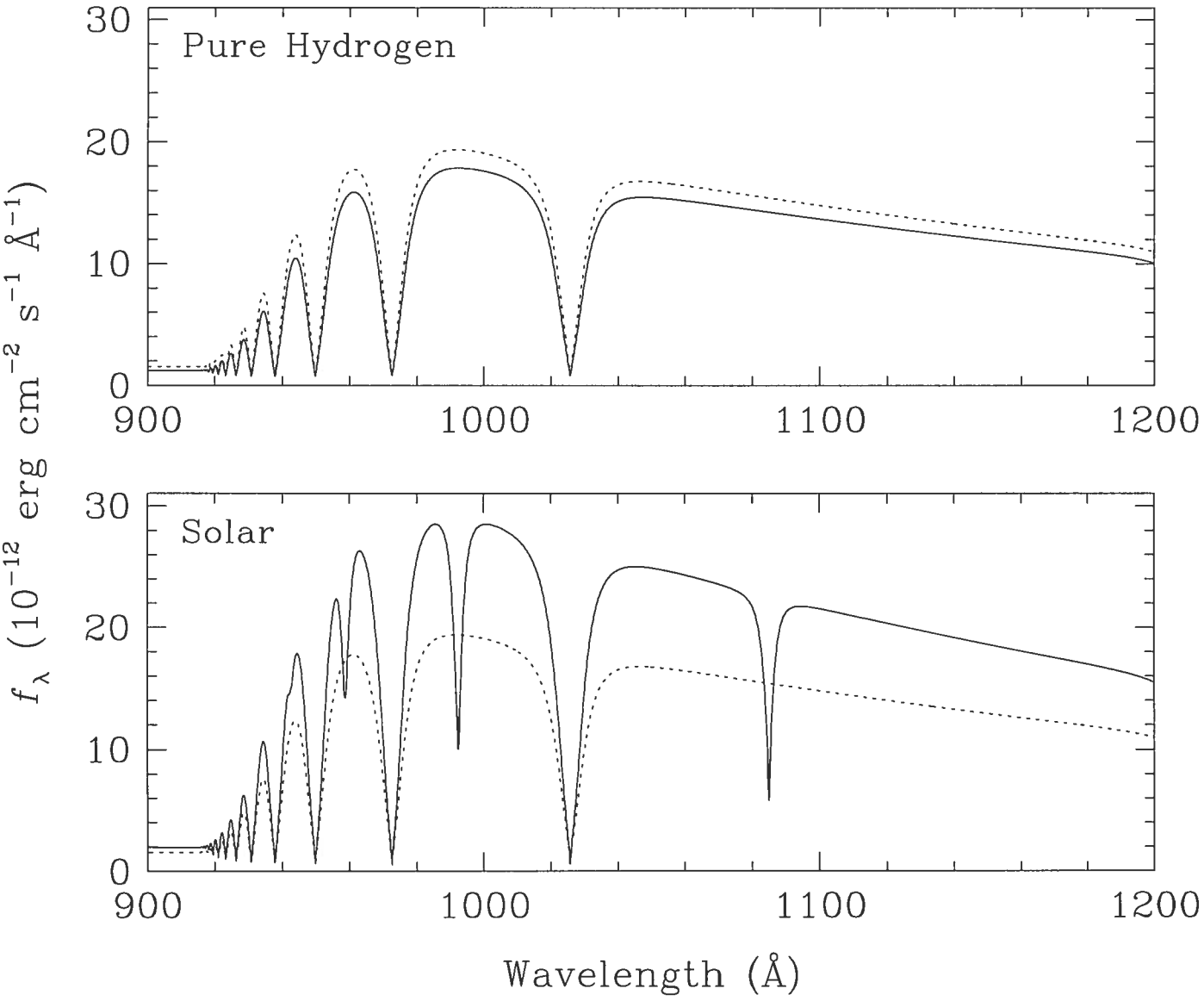

FIGURE 3.11 – Top panel: Superposition of a pure hydrogen model ($T_{\rm eff}$ = 34,000 K, $\log g = 6.0$) computed with TLUSTY (dashed line) and one calculated with STERNE (solid line). Bottom panel: Superposition of a pure hydrogen model ($T_{\rm eff}$ = 34,000 K, $\log g = 6.0$) computed with TLUSTY (dashed line) and one calculated with STERNE (solid line) of solar metal abundance. We see that unlike the Balmer line profiles, that are only slightly affected by the presence of heavy elements, the Lyman line profiles in the FUV region are narrower and the flux level higher.

Chapitre 4

Conclusion

Nous avons présenté deux études spectroscopiques de deux classes d'étoile comportant certaines similitudes. La spectroscopie s'est avérée un outil fort utile en nous donnant accès à une importante quantité d'information sur les atmosphères de ces objets évolués et compacts.

Dans le cas de GD 323, la question de la variabilité spectroscopique a été étudiée. En examinant les largeurs équivalentes des raies d'hydrogène et d'hélium de spectres obtenus au cours de cinq nuits, nous avons détecté des variations dans ces raies d'absorption. Dans le cas de Hβ, par exemple, nous détectons des variations de 30%. Bien que ce résultat soit remarquable, ce qui est encore plus surprenant est le fait que les raies d'hydrogène varient hors-phase avec la raie la plus forte de l'hélium, He λ4471. De plus, ces variations semblent être quasi-périodiques avec une période d'environ 3.5 heures. Cette valeur est en accord avec la période typique de rotation des naines blanches.

Cette découverte a plusieurs implications. En premier lieu, cela indique que le modèle favorisé jusqu'à présent, soit celui d'une atmosphère stratifiée, n'est plus valide. C'est plutôt le modèle d'une atmosphère avec des abondances inhomogènes qui représente le mieux les variations. Des calculs de ce type effectués par Beauchamp et al. (1993) supposent une géométrie avec une ceinture d'hélium et des calottes d'hydrogène. Les flux émergents prédits dans cette étude dépendent de la taille de la ceinture d'hélium, ainsi que de l'angle entre l'axe de symétrie de l'étoile et la ligne de visée. Nous voyons que malgré les différences évidentes entre les modèles et les observations, des calculs plus rafinés pourraient améliorer l'accord entre les prédictions

et les observations.

Nous proposons comme explication pour ces abondances inhomogènes la dilution de l'enveloppe d'hydrogène par mélange convectif. Les modèles évolutifs des naines blanches suggèrent qu'un tri gravitationnel sépare l'hydrogène et l'hélium de façon à ce qu'on ne retrouve que des naines blanches de type DA entre 45,000 K et 30,000 K. Cette région se nomme la brèche des DB, étant donné qu'on n'y détecte aucune étoile avec des atmosphères riches en hélium. Cependant, autour de 30,000 K, la convection vient contrer l'effet du tri gravitationnel, et une DA pourrait alors se transformer en DB. Il se trouve que GD 323 a une température autour de cette limite. Or, si cette transformation se produit, on serait en mesure d'expliquer les inhomogénéités d'abondance observées dans GD 323. Toutefois, nos connaissances sur cette hypothèse demeurent limitées. Par conséquent, il sera nécessaire d'étudier ce processus plus en détail avant que l'on puisse vraiment comprendre GD 323.

Du côté de notre analyse des sous-naines, nous avons montré qu'il existe un bon accord lorsqu'on compare les paramètres dérivés à partir de spectres visibles avec les observations dans l'ultraviolet lointain. À première vue, nous remarquons une cohérence dans les résultats pour les objets à basse température ($T_{\rm eff} < 27,000$ K) dans notre échantillon. Pour les objets à plus haute température, il semble y avoir une moins bonne cohérence. En conséquence, nous avons exploré diverses explications pour aboutir à un bon accord entre les modèles et les observations.

Le premier facteur ayant des implications importantes est la question du rougissement interstellaire. Dans le cas de quatre de nos objets, PHL 457, PG 1743+477, PG 1710+490 et PG 0823+466, des étoiles ayant toutes des températures effectives entre 27,000 K et 31,000 K, nous trouvons qu'une correction due au rougissement est nécessaire et permet d'obtenir un meilleur accord. Nous trouvons des valeurs de $E(B-V)$ de 0.02, 0.03, 0.02 et 0.07, respectivement. Ces valeurs, même si elles sont faibles, ont un impact observable sur nos résultats. Le profil des raies de Lyman et le continu sont mieux reproduits lorsqu'on corrige pour cet effet.

Par contre, une incohérence persiste pour nos objets à plus haute température ($T_{\rm eff} > 31,000$ K). Nous avons été amenés à chercher d'autres explications. Par exemple, nous avons

exploré les effets des éléments lourds sur les modèles d'atmosphères. Nous trouvons que l'inclusion d'éléments lourds avec une abondance solaire a une influence plus prononcée dans le calcul de spectres de l'ultraviolet lointain que dans celui du visible. En effet, un spectre synthétique calculé à partir d'un modèle d'hydrogène pur ne diffère pas beaucoup de celui calculé à partir d'un modèle riche en éléments lourds dans la région des raies de Balmer. Par contre, la situation s'inverse dans la région de l'ultraviolet lointain. Le profil des raies de Lyman ainsi que le continu sont grandement affectés par la présence d'éléments lourds. Notamment, nous trouvons des raies plus étroites et un niveau du continu plus élevé pour un modèle d'abondance solaire que pour un modèle d'hydrogène pur. Ce comportement est en accord avec les observations des spectres *FUSE*. Nous suggérons donc que le désaccord observé dans les objets chauds peut s'expliquer par la présence d'éléments lourds dans la photosphère. Cependant, nous disposons uniquement d'un modèle à une seule température effective. Il serait intéressant d'examiner si cet effet est présent à toutes les températures, ou s'il est important uniquement à haute température. Par ailleurs, nous avons seulement fait l'expérience avec un modèle ayant un abondance solaire. Nous savons que, dans le cas des sous-naines, les abondances des éléments lourds varient d'objet en objet. Il serait donc très intéressant de vérifier l'impact des éléments lourds pour les variations d'abondances caractéristiques de ce type d'étoile. De plus, la méthode développée dans cette étude serait utile dans les analyses d'abondances des spectres *FUSE*, où il est souvent difficile de bien définir l'emplacement du continu à cause de la présence de nombreuses raies d'éléments lourds.

Il reste donc à calculer des grilles complètes de modèles qui incluent les éléments lourds. Seulement lorsque cela sera accompli, serons nous en mesure de mieux vérifier la compatibilité entre les deux régions spectrales.

Bibliographie

Achilleos, N., Wickramasinghe, D. T., Liebert, J., Saffer, R. A., & Grauer, A. D. 1992, ApJ, 396, 273

Angel, J. R. P., Borra, E. F., & Landstreet, J. D. 1981, ApJS, 45, 457

Barstow, M. B., Good, S. A., Burleigh, M. R., Hubeny, I., Holberg, J. B., & Levan, A. J. 2003, MNRAS, 334, 562

Barstow, M. B., Holberg, J. B., Hubeny, I., Good, S. A., Levan, A. J., & Meru, F. 2001, MNRAS, 328, 211

Beauchamp, A., Wesemael, F., Fontaine, G., & Bergeron, P. 1993, in White Dwarfs: Advances in Observation and Theory, Vol. 403, 281

Bergeron, P., Fontaine, G., Lacombe, P., Wesemael, F., Crawford, D. L., & Jakobsen, A. M. 1984, AJ, 89, 374

Bergeron, P. & Liebert, J. 2002, ApJ, 566, 1091

Bergeron, P., Saffer, R. A., & Liebert, J. 1992, ApJ, 394, 228

Bergeron, P., Wesemael, F., Michaud, G., & Fontaine, G. 1988, ApJ, 332, 964

Brown, T. M., Ferguson, H. C., & Davidsen, A. F. 1996, ApJ, 472, 327

Burleigh, M., Bannister, N., & Barstow, M. 2001, in 12th European Workshop on White Dwarfs, Vol. 226, 135

Burstein, D. & Heiles, C. 1982, AJ, 87, 1165

D'Cruz, N. L., Dorman, B., Rood, R. T., & O'Connell, R. W. 1996, ApJ, 466, 359

Dufour, P., Wesemael, F., & Bergeron, P. 2002, ApJ, 575, 1025

Edelmann, H., Heber, U., Hagen, H.-J., Lemke, M. nd Dreizler, S., Napiwotzki, R., & Engels, D. 2003, A&A, 400, 939

Fontaine, G. & Chayer, P. 1997, in The Third Conference on Faint Blue Stars, 169

Fontaine, G. & Wesemael, F. 1987, in The Second Conference on Faint Blue Stars, Vol. 95, 319

Fontaine, M., Chayer, P., Wesemael, F., Lamontagne, R., Blanchette, J.-P., & Fontaine, G. 2005, in Astrophysics in the Ultraviolet, in press

Good, S. A., Barstow, M. B., Holberg, J. B., Sing, D. K., Burleigh, M. R., & Dobbie, P. D. 2004, MNRAS, 355, 1031

Han, Z., Podsiadlowski, P., Maxted, P. F. L., & Marsh, T. R. 2003, MNRAS, 341, 669

Han, Z., Podsiadlowski, P., Maxted, P. F. L., Marsh, T. R., & N., I. 2002, MNRAS, 336, 449

Heber, U. 1986, A&A, 155, 33

Heber, U., Napiwotzki, R., Lemke, M., & Edelmann, H. 1997a, A&A, 324, L53

Heber, U., Napiwotzki, R., & Reid, I. N. 1997b, A&A, 323, 819

Holberg, J. B., Kidder, K. M., & Wesemael, F. 1990, ApJ, 365, L77

Holberg, J. B., Wesemael, F., Wegner, G., & Bruhweiler, F. C. 1985, ApJ, 293, 294

Hubeny, I. 1988, Computer Physics Comm., 52, 103

Hubeny, I. & Lanz, T. 1995, ApJ, 439, 875

Iben, I. J. & Tutukov, A. V. 1986, ApJ, 311, 735

Jeffery, C. S. & Heber, U. 1992, A&A, 260, 133

Jordan, S., Heber, U., Engels, D., & Koester, D. 1993, A&A, 273, L27

Karl, C., Napiwotzki, R., Heber, U., Dreizler, S., Koester, D., & Reid, I. N. 2005, A&A, 434, 637

Kidder, K. M., Holberg, J. B., Barstow, M. A., Tweedy, R. W., & Wesemael, F. 1992, ApJ, 394, 288

Kilkenny, D., Heber, U., & Drilling, J. S. 1988, South African Astron. Obs. Circ., 12, 1

Kilkenny, D., Hill, P. W., & Brown, A. 1977, MNRAS, 178, 123

Koester, D. 1991a, in Evolution of Stars: The Photospheric Abundance Connection, Vol. 145, 435

Koester, D. 1991b, in White Dwarfs, Vol. 336, 343

Koester, D., Liebert, J., & Saffer, R. A. 1994, ApJ, 422, 783

Lanz, T. & Hubeny, I. 2003, ApJS, 146, 417

Lanz, T., Hubeny, I., & Reap, S. R. 1997, ApJ, 485, 843

Lemke, M. 1997, A&A, 122, 285

Liebert, J., Bergeron, P., & B., H. J. 2005, ApJS, 156, 47

Liebert, J., Fontaine, G., & Wesemael, F. 1987, Mem. Soc. Astr. Italiana, 58, 17

Liebert, J., Wesemael, F., Sion, E. M., & G., W. 1984, apj, 277, 692

Maxted, P. F. L., Burleigh, M. R., Marsh, T. R., & Bannister, N. P. 2002, MNRAS, 334, 833

Maxted, P. F. L., Heber, U., Marsh, T. R., & North, R. C. 2001, MNRAS, 326, 1391

Mccook, G. P. & Sion, E. M. 1999, ApJS, 121, 1

Michaud, G., Bergeron, P., Heber, U., & Wesemael, F. 1988, ApJ, 338, 417

Moehler, S., Heber, U., & deBoer, K. S. 1990, A&A, 239, 265

Moos, H. W. e. a. 2000, ApJ, 538, L1

Napiwotzki, R. 1997, A&A, 322, 256

Napiwotzki, R. & the SPY Consortium. 2005, in 14th European Workshop on White Dwarfs, Vol. 334, 375

Ohl, R. G., Chayer, P., & Moos, H. W. 2000, ApJ, 538, L95

Oke, J. B., Weidemann, V., & Koester, D. 1984, ApJ, 281, 276

Robinson, E. L. & Winget, D. E. 1983, PASP, 95, 386

Saffer, R. A., Bergeron, P., Koester, D., & Liebert, J. 1994, ApJ, 432, 351

Sahnow, D. J. e. a. 2000, ApJ, 538, L7

Seaton, M. J. 1979, MNRAS, 187, 73P

Sweigart, A. V. 1997, ApJ, 474, L23

Unglaub, K. & Bues, I. 2001, A&A, 374, 570

Vennes, S., Chayer, P., Dupuis, J., & Lanz, T. 2005, in 14th European Workshop on White Dwarfs, 185

Vennes, S., Dupuis, J., & Chayer, P. 2004, ApJ, 611, 1091

Wesemael, F., Bergeron, P., & E., B. 1995, JRASC, 89, 183

Wesemael, F., Bergeron, P., Lamontagne, R., Fontaine, G., Beauchamp, A., Demers, S., Irwin, M. J., Holberg, J. B., Kepler, S. O., & Vennes, S. 1994, ApJ, 429, 369

Wesemael, F., Fontaine, G., Bergeron, P., Lamontagne, R., & Green, R. F. 1992, AJ, 104, 203

Wesemael, F., Greenstein, J. L., Liebert, J., Lamontagne, R., Fontaine, G., Bergeron, P., & Glaspey, J. W. 1993, PASP, 105, 761

Wolff, B., Jordan, S., Koester, D., & Reimers, D. 2000, A&A, 361, 629

Remerciements

J'aimerais remercier Pierre Bergeron et François Wesemael pour leur support et leur encouragement.

Je remercie également Patrick Dufour, Mathieu Fontaine, Alexandros Gianninas, Charles-Philippe Lajoie, Delphine Quievy et Suzanna Randall pour leur aide et leur patience.